AD_____

Award Number: DAMD17-02-1-0628

TITLE: Diagnosis of Breast Cancer Using Fluorescence and Reflectance Spectroscopy

PRINCIPAL INVESTIGATOR: Gregory M. Palmer
Nirmala Ramanujam, Ph.D.

CONTRACTING ORGANIZATION: University of Wisconsin-Madison
Madison, Wisconsin 53706-1490

REPORT DATE: September 2003

TYPE OF REPORT: Annual Summary

PREPARED FOR: U.S. Army Medical Research and Materiel Command
Fort Detrick, Maryland 21702-5012

REPORT DOCUMENTATION PAGE

Form Approved
OMB No. 074-0188

1. AGENCY USE ONLY (Leave blank)	2. REPORT DATE	3. REPORT TYPE AND DATES COVERED
	September 2003	Annual Summary (1 Sep 2002 - 31 Aug 2003)

4. TITLE AND SUBTITLE
Dianosis of Breast Cancer Using Fluorescence and Reflectance Spectroscopy

5. FUNDING NUMBERS
DAMD17-02-1-0628

6. AUTHOR(S)
Gregory M. Palmer
Nirmala Ramanujam, Ph.D.

7. PERFORMING ORGANIZATION NAME(S) AND ADDRESS(ES)
University of Wisconsin-Madison
Madison, Wisconsin 53706-1490

E-Mail: greg-palmer@usa.net

8. PERFORMING ORGANIZATION REPORT NUMBER

9. SPONSORING / MONITORING AGENCY NAME(S) AND ADDRESS(ES)
U.S. Army Medical Research and Materiel Command
Fort Detrick, Maryland 21702-5012

10. SPONSORING / MONITORING AGENCY REPORT NUMBER

11. SUPPLEMENTARY NOTES

12a. DISTRIBUTION / AVAILABILITY STATEMENT
Approved for Public Release; Distribution Unlimited

12b. DISTRIBUTION CODE

13. ABSTRACT (Maximum 200 Words)

The goal of this grant is to characterize the fluorescence and diffuse reflectance properties of breast tissue, and identify features in the spectra which may be useful in diagnosing breast cancer. In the past 12 months in which the award was active, 3 reviewed manuscripts have been accepted for publication, and two conference presentations have been completed. Significant work includes characterization of the intrinsic fluorescence properties of normal and malignant human breast cell lines. It was found that the malignant cell lines have significantly different fluorescence properties for the fluorophores, tryptophan, and NAD(P)H. This suggests that these fluorophores could be important indicators of malignancy in tissue, and could be exploited in an in vivo diagnostic device. Additional work has focused on completion of a preliminary investigation to characterize fluorescence and diffuse reflectance properties in human breast tissue, and development of analysis techniques for interpreting spectral data.

14. SUBJECT TERMS
Fluorescence, reflectance, breast cancer, diagnosis, cell culture

15. NUMBER OF PAGES
26

16. PRICE CODE

17. SECURITY CLASSIFICATION OF REPORT	18. SECURITY CLASSIFICATION OF THIS PAGE	19. SECURITY CLASSIFICATION OF ABSTRACT	20. LIMITATION OF ABSTRACT
Unclassified	Unclassified	Unclassified	Unlimited

Table of Contents

Introduction:

Our goal is to develop a diagnostic device for breast cancer based on fluorescence and diffuse reflectance spectroscopy. Our specific objectives are to characterize the fluorescence properties of normal, benign, and malignant breast tissue in patients undergoing breast cancer and breast reduction surgeries. Additionally, we will characterize the intrinsic fluorescence properties of tissue constituents in order to identify the biological basis for spectral differences in tissue. An initial, *ex vivo*, study will be completed, and then a fast, portable device will be employed to measure the fluorescence and diffuse reflectance properties of tissue, *in vivo*. Results will be correlated with the gold standard, histopathology, to develop statistical methods to determine the diagnostic potential of this technology.

Body:

The first major focus of work over the past 12 months has been in identifying the biological basis for the effectiveness of fluorescence spectroscopy in diagnosing breast cancer. To this end, the fluorescence properties of one normal and four malignant cell lines were characterized using fluorescence spectroscopy. Specifically, the fluorescence properties of three intrinsic fluorophores: tryptophan, nicotinamide adenine dinucleotide (NAD(P)H), and flavin adenine dinucleotide (FAD), were characterized using fluorescence spectroscopy. Additionally, two-photon excitation microscopy was employed to image NAD(P)H fluorescence from the normal and one of the malignant cell lines. It was found that the fluorescence intensity of tryptophan and NAD(P)H were significantly reduced in the malignant cell lines ($p < 0.05$). A manuscript detailing these

results and their implications has been accepted into the peer-reviewed journal, *Photochemistry and Photobiology*, and is included in Appendix A (p.6). This work addresses part (a) of Task 1 in the Statement of Work.

Parts (b-c) of Task 1 in the statement of work involve the measurement of fluorescence and diffuse reflectance spectra of human breast tissues, *ex vivo*. Unfortunately, some difficulty was encountered in gaining approval for conducting human subjects research from the DOD Institutional Review Board. Approval has recently been obtained, however, and we plan to proceed with collection of this data in the coming year. This has delayed the start of our study, but should not affect our overall goals.

A preliminary study involving another protocol not covered under this grant was completed however, and serves to answer some of the questions posed by Task 1 of the Statement of Work. A comparison of classification accuracy using empirically-based statistical methods was carried out. Fluorescence and diffuse reflectance properties of breast tissue was characterized for a total of 56 samples from 32 patients, immediately after surgery. To briefly summarize, it was found that fluorescence-based detection of breast cancer was highly successful, with a cross-validated classification accuracy of 84%. It was found that diffuse reflectance-based detection of breast cancer was less effective, with a cross validated classification accuracy of 61%. A manuscript detailing the results of this study was accepted for publication into the peer-reviewed journal, *IEEE Transactions on Biomedical Engineering* and is included in Appendix B (p. 14).

One limitation of this study is that it employed a fixed probe geometry, with a central bundle of optical fibers for collection of light, and an outer ring of illumination

fibers. Furthermore, little research has been done to identify how probe geometry affects the diagnostic efficacy of these methods. The study to be completed under this grant's protocol will be carried out using a probe designed with multiple separation distances between the illumination and collection fibers. A schematic of this probe design is shown in Fig. 1. Because the probe geometry affects the probing volume within the tissue [1], having multiple probing geometries will allow us to evaluate in what way probe geometry affects the information content obtained with these measurements, and will also help determine if there is an optimal probe geometry for use in future studies.

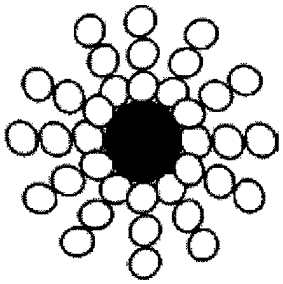

Fig. 1: Probe geometry to be used in the current human subjects protocol. The probe consists of a central illumination region (black) surrounded by three concentric rings of collection fibers.

Part (d) of Task 1 pertains to developing a method of analysis for interpreting spectral data taken from the tissue specimens. To this end a novel statistical method of analysis, appropriate for small sizes, has been developed and tested on spectral data obtained from the preliminary *ex vivo* breast tissue study. This method is described in detail in the manuscript submitted in Appendix B (p. 14), and will be applied to future data collected in this study.

Key Research Accomplishments

- Identification of intrinsic differences in fluorescence properties of human breast cell cultures with malignancy

- Identification of spectral differences present in human breast tissue, *ex vivo*.
- Development of a statistical method of analysis for evaluating the classification accuracy of optical spectroscopy in diagnosing breast cancer

Reportable Outcomes:

Degrees Obtained:

Master's of Science – Biomedical Engineering, Dec. 2002

Journal Articles:

- Palmer, G.M., C. Zhu, T.M. Breslin, F. Xu, K.W. Gilchrist, and N. Ramanujam. "Comparison of multi-excitation fluorescence and diffuse reflectance spectroscopy for the diagnosis of breast cancer, ex vivo." Accepted, IEEE Trans BME.
- Breslin, T.M., F. Xu, G.M. Palmer, C. Zhu, K.W. Gilchrist, and N. Ramanujam. "Auto fluorescence and diffuse reflectance properties of malignant and benign breast tissues." Accepted, Ann. Surg. Onc.
- Palmer, G.M., P.J. Keely, T.M. Breslin, and N. Ramanujam. "Autofluorescence spectroscopy of normal and malignant human breast cell lines." Accepted, Photochem Photobiol.

Conference Presentations:

- Palmer, G.M., C. Zhu, T.M. Breslin, P.J. Keely, F. Xu, K.W. Gilchrist, J.M. Squirrell, J.G. White, and N. Ramanujam. "Use of auto fluorescence and diffuse reflectance spectroscopy for the diagnosis of breast cancer, ex vivo, and its biological basis." *Poster Presentation*, Third Inter-Institute Meeting on

Diagnostic Optical Imaging and Spectroscopy: The Clinical Adventure. National Institutes of Health, Bethesda, MD, Sept. 2002.

- Palmer, G.M., P.J. Keely, T.M. Breslin, J.M. Squirrell, J.G. White, and N. Ramanujam. "Understanding Sources of Contrast in Fluorescence Based Diagnosis of Breast Cancer." *Poster Presentation*, Engineering Conferences International: Advances in Optics. Banff, Canada. Aug. 2003.

Conclusions

Significant differences in the fluorescence and diffuse reflectance properties of normal and malignant breast tissues have been identified, and a method for classification of these tissues has been developed. A diagnostic device based on fluorescence and diffuse reflectance spectroscopy has the advantage of being fast, quantitative, and minimally invasive, and could improve breast cancer care both in assessing surgical margins for residual cancer *in vivo* during surgery, as well as during core needle biopsy to accurately identify the appropriate region to biopsy. Furthermore, the biological basis for observed differences in fluorescence properties of the tissue has been examined, and differences in the intrinsic fluorescence properties of normal and malignant human breast cell lines have been identified. These differences in intrinsic cellular fluorescence could explain, in part, the biological basis for observed spectral differences in tissue.

References

1. Zhu, C., Q. Liu, and N. Ramanujam, *Effect of fiber optic probe geometry on depth-resolved fluorescence measurements from epithelial tissues: a Monte Carlo simulation.* J Biomed Opt, 2003. **8**(2): p. 237-47.

Photochemistry and Photobiology, 2003, 78(5): 000–000

Autofluorescence Spectroscopy of Normal and Malignant Human Breast Cell Lines¶

Gregory M. Palmer[1], Patricia J. Keely[2], Tara M. Breslin[3] and Nirmala Ramanujam*[1]

[1]Department of Biomedical Engineering, University of Wisconsin, Madison, WI;
[2]Department of Pharmacology, University of Wisconsin, Madison, WI and
[3]Department of Surgery, University of Wisconsin, Madison, WI

Received 21 January 2003; accepted 10 August 2003

ABSTRACT

The fluorescence of tryptophan, reduced nicotinamide adenine dinucleotide (phosphate) (NAD(P)H) and flavin adenine dinucleotide (FAD) were characterized in normal human breast cells as well as in malignant human breast cells of similar and dissimilar genetic origins. Fluorescence measurements of each cell line were made over a wide range of cell concentrations, and the fluorescence per cell was determined from the slope in the linear range of the fluorescence intensity *vs* cell concentration plot. All of the malignant cells showed a statistically significant decrease in the tryptophan fluorescence per cell relative to that of the normal cells. No statistically significant differences were observed in the NAD(P)H or FAD fluorescence per cell between the normal and any of the malignant cell types. NAD(P)H fluorescence was also imaged from monolayers of the normal and malignant cells (of similar genetic origin) using two-photon fluorescence microscopy. A statistically significant decrease in the NAD(P)H fluorescence with malignancy was observed, suggesting that fluorescence imaging of single cells or the cell monolayer preparation may provide more contrast than volume-averaged fluorescence measurements of cells in suspension. In conclusion, the differences in normal and malignant human breast tissue fluorescence spectra may be attributed in part to differences in the intrinsic cellular fluorescence of normal and malignant breast epithelial cells.

INTRODUCTION

Breast cancer screening relies on mammography, which is effective in identifying suspicious lesions. However, a significant number of false positives are produced (1). As a result, follow-up diagnostic procedures such as percutaneous core needle biopsy with image guidance are performed to further evaluate these abnormalities (1). Core needle biopsy has a limited sampling accuracy because only a few small pieces of tissue are extracted from random locations in the suspicious mass. In some cases, the suspicious mass may be missed altogether.

Optical sensors based on ultraviolet–visible (UV–VIS) spectroscopy have the potential to improve the sampling accuracy of core needle biopsy. Optical techniques have the capability to survey multiple tissue sites without the need for biopsy and provide real-time diagnosis. UV–VIS fluorescence spectroscopy is a technique that has been shown to have consistently high sensitivities and specificities for detecting human precancers and early cancers *in vivo* in a number of organ sites, including the gastrointestinal tract, bronchus and cervix (2). Incorporating UV–VIS fluorescence spectroscopy as an adjunct diagnostic modality to image-guided core needle biopsy could potentially reduce the false-negative rate of current breast biopsy procedures. This in turn could lead to fewer follow-up procedures and fewer repeat biopsies in patients suspected to have breast cancer. A second potential application of UV–VIS fluorescence spectroscopy is the evaluation of tumor margins during breast cancer surgery. A real-time, accurate means of assessing tumor margins could reduce intraoperative time as well as provide greater assurance that the entire lesion has been removed.

Breast tissue, which is primarily composed of epithelial cells, an extracellular matrix and fat, contains a number of endogenous fluorophores. Tryptophan, reduced nicotinamide adenine dinucleotide (phosphate) (NAD(P)H) and flavin adenine dinucleotide (FAD) are present in the epithelial cells (3–6). The excitation–emission maxima corresponding to the peaks of these fluorophores are 280–340 nm for tryptophan, 340–460 nm for NAD(P)H and 460–520 nm for FAD (3–6). Tryptophan accounts for the majority of protein fluorescence, and its emission is sensitive to the polarity of the environment (7). NAD(P)H and FAD are involved in the oxidation of fuel molecules and can be used to probe changes in cellular metabolism (8). The primary fluorophore in the breast tissue extracellular matrix is type I collagen (9), which has a peak near 330–400 nm that is attributed to cross-links (4). Other major factors that influence breast tissue fluorescence spectra in the UV–VIS spectrum are endogenous absorbers and scatterers in the tissue. Absorption in tissue is dominated by oxygenated and deoxygenated hemoglobin (10). Scattering occurs because of local changes in the index of refraction across mitochondrial and other membrane interfaces (10). Wavelength-dependent absorption and scattering

---

¶Posted on the website on

*To whom correspondence should be addressed at: Department of Biomedical Engineering, University of Wisconsin, Room 2144, 1550 Engineering Drive, Madison, WI 53706, USA. Fax: 608-265-9239; e-mail: nimmi@engr.wisc.edu

Abbreviations: DMEM, Dulbecco modified Eagle medium; EEM, excitation–emission matrices; FAD, flavin adenine dinucleotide; NAD(P)H, reduced nicotinamide adenine dinucleotide (phosphate); PBS, phosphate-buffered saline; PMT, photomultiplier tube; UV–VIS, ultraviolet–visible.

affect both the spectral intensity and the line shape of the fluorescence measured from the tissue.

Several groups have demonstrated that there are significant differences in the fluorescence excitation and emission spectra of normal, benign and malignant breast tissues *ex vivo* (11–17). However, it is difficult to directly interpret the sources of endogenous fluorescence contrast between the malignant and nonmalignant breast tissues from the measured tissue fluorescence spectra. This is due to the complex interplay of fluorescence, absorption and scattering. Thus, systematic investigations of breast tissue constituent fluorescence in progressively complex biological systems that range from cells to tissue cultures to living animal models of breast cancer may provide an effective approach toward understanding the differences in the endogenous fluorescence of malignant and nonmalignant breast tissues.

Several groups have characterized the fluorescence of normal and malignant cells for a number of cell types (5,18–22). Thus far, only one group has studied the fluorescence properties of normal and malignant human breast cells (22). Glassman *et al.* (22) measured fluorescence from the normal HTB125 and the malignant HTB22 and HTB126 human breast cells (American Type Culture Collection, Rockville, MD). The HTB125 and HTB126 were derived from the same patient. Fluorescence spectra were recorded at an excitation wavelength of 353 nm from cells that were centrifuged and then packed into a cuvette. The results showed that the NAD(P)H fluorescence of the malignant cells is a factor of 2 higher than that of normal cells at this excitation wavelength. The observed increase in NAD(P)H fluorescence was attributed to the increased metabolic rate of the malignant cells.

These results set an important precedent for future work. However, there are a number of potential refinements that can be incorporated into future studies that will improve the quality and information content of cellular fluorescence measurements. This includes (1) the comparison of normal and malignant cell phenotypes of genetically similar origins; (2) characterization of all the endogenous fluorophores present in these cells; (3) measurement of cellular fluorescence at concentrations at which the effects of turbidity are minimal; and (4) viability testing before and after the experimental measurements.

The goal of this work was to systematically characterize the differences in the fluorescence properties of normal and malignant human breast cell lines. This study builds upon previous work and attempts to minimize potential sources of error that can influence the analysis and interpretation of fluorescence measurements from cells. Measurements were made from suspensions of breast cells to allow for the characterization of fluorescence from a relatively simple biological system of the normal breast and breast cancer cells. In this system, there was no direct cell to cell or cell to extracellular matrix interaction. These effects, which are important for cell signaling, are evaluated to a limited extent and will be evaluated more thoroughly in an independent study that includes cell monolayers and tissue cultures (see Discussion). These stepwise investigations will enable a systematic comparison of the effects of different microenvironments on the fluorescence properties of normal and malignant human breast cells.

Three cell lines were used in these studies. These included the well-differentiated T47D cells and the poorly differentiated MDA231 cells, which are both spontaneously occurring human breast adenocarcinomas, and the MCF10 cell line, which is a putatively normal human breast cell line. The T47D cell line was derived from a 54-year-old patient with infiltrating ductal carcinoma (23). The MDA231 cell line was derived from a 51-year-old woman with cancer that had developed a plural effusion (24). Finally, the MCF10 cell line was derived from benign mastectomy tissue obtained from a 36-year-old woman (25). These cells became spontaneously immortalized in culture into a nontumorigenic, putatively normal cell line (25). To compare normal and malignant phenotypes of similar genetic origins, MCF10 cells were transformed by stable expression of the R-Ras oncogene (malignant phenotype) or transfected with only the pZIP vector (normal phenotype). Although the immortalized MCF10 cells may not be "truly normal," transforming these cells with the R-Ras oncogene enables a direct comparison between transformed cells (with a known oncogene) and their nontransformed counterpart. In addition, the T47D cell line was stably transfected with the R-Ras oncogene to serve as a positive control because a normal to malignant transformation is not expected in these cells.

Fluorescence spectra of suspensions from each cell type (from a total of five cell types) were measured over the entire UV–VIS range to characterize the fluorescence of all three endogenous fluorophores, tryptophan, NAD(P)H and FAD, present in the cells. For each cell type, the fluorescence measurements were carried out over a range of cell concentrations, and the fluorescence per cell was determined from the slope in the linear range of the fluorescence intensity *vs* cell concentration plot. Cell viability was determined before and after each experiment. In addition, the cell sizes were quantitatively determined for each cell type.

All of the malignant cells showed a statistically significant decrease in the tryptophan fluorescence per cell relative to that of the normal cells. No statistically significant differences were observed in the NAD(P)H or FAD fluorescence per cell between the normal and any of the malignant cell types. The tryptophan fluorescence per cell was found to be very similar for the T47D and T47D R-Ras (positive control) cell lines, confirming that the differences in the tryptophan fluorescence of the nontransformed MCF10 pZIP cells and the transformed MCF10 R-Ras cells are not due to the expression of the R-Ras oncogene but rather due to the transformation of the MCF10 cells from a normal to a malignant phenotype. In addition, cell viability (greater than 80%) and cell sizes (150–200 μm^2) were found to be similar for all cell lines evaluated in this study.

NAD(P)H fluorescence was also imaged from monolayers of the normal and malignant cells (of similar genetic origin) using two-photon fluorescence microscopy. A statistically significant decrease in the NAD(P)H fluorescence with malignancy was observed, suggesting that fluorescence imaging of single cells or the cell monolayer preparation may provide more contrast than volume-averaged fluorescence measurements of cells in suspension.

MATERIALS AND METHODS

Preparation of cell suspensions. Cell lines were obtained from the American Type Culture Collection and were maintained free of mycoplasma or other contamination by adherent culture according to their individual established protocols. Measurements were made on cells having passage numbers of 50 or less. The cells were not synchronized. The T47D cells were grown in Roswell Park Memorial Institute 1640 medium supplemented with 10% fetal bovine serum and 8 μg/mL insulin. The MDA231 cells were grown in Dulbecco modified Eagle media (DMEM)–F12 supplemented with 10% horse serum. The MCF10 cells were grown in DMEM–F12 supplemented with 5% horse serum, 10 μg/mL insulin, 20 ng/mL epidermal growth factor and 0.5 μg/mL hydrocortisone. Cells were incubated at 37°C with 5% CO_2 for the T47D cells and 10% CO_2 for the MDA231 and MCF10 cells. Transfection of the MCF10 and T47D cells

with the R-Ras oncogene was performed according to previously described protocols (26).

Upon reaching confluence (generally 3–4 days after plating), the cells were detached from their plates by trypsinization and triply washed in phosphate-buffered saline (PBS). This was carried out using 10 mL of PBS per wash. After the final wash, the cells were resuspended in a final volume of 3 mL PBS. Cell concentration was determined by counting the number of cells per milliliter using a hemacytometer. This measurement was repeated four times (by making an independent count in each of the four grids in the hemacytometer) to obtain a standard deviation of the concentration of cells. The solution containing the cells was then diluted to attain the experimental concentration. Cell suspensions at approximately eight concentrations (5×10^5 cells/mL to 3×10^6 cells/mL), each taken from an independent cell culture, were characterized for each cell line.

The viability was visually evaluated by checking membrane integrity using a phase-contrast stereomicroscope. This process was repeated four times (again using each of the four hemacytometer grids) to obtain a standard deviation for cell viability. The accuracy of determining cell viability by sight with a phase-contrast microscope was compared with a trypan blue exclusion assay (gold standard). The viability assays using phase-contrast microscopy and the trypan blue assay were carried out 12 times (four repetitions at each of three different concentrations) from a T47D cell culture over a range of concentrations within the experimental concentration range (5×10^5 cells/mL to 3×10^6 cells/mL). The average viability determined by phase-contrast microscopy and the trypan blue assay was $87.5 \pm 5.9\%$ and $88.1 \pm 7.6\%$, respectively. A Wilcoxon rank-sum test (27) was used to confirm that the differences in cell viability obtained with the two methods are statistically insignificant ($P > 0.5$).

Fluorescence spectroscopy of cell suspensions. The cell suspension was placed in a 1 cm path length quartz cuvette. A conventional laboratory fluorometer (Fluorolog-3, JY Horiba Inc., Edison, NJ) was used to characterize the fluorescence properties of each cell suspension. The instrument consists of a 450 W xenon arc lamp, double excitation and emission scanning monochromators, a sample compartment with a cuvette holder and magnetic stirrer and a photomultiplier tube (PMT). Adjustable parameters include the excitation and emission wavelength ranges and increment, the excitation and emission band-passes, the high voltage of the PMT, the integration time, the stirring speed of the magnetic stirrer and the collection geometry (right angle or front face).

Fluorescence excitation–emission matrices (EEM) were recorded by measuring the fluorescence emission spectra over a range of excitation wavelengths. A fluorescence EEM involves measurement of the fluorescence intensity as a function of both excitation and emission wavelengths. The excitation wavelength was varied from 260 to 540 nm in 20 nm increments. At each excitation wavelength, the fluorescence emission spectra were recorded from 275 to 700 nm in 5 nm increments. These wavelength ranges enabled characterization of all endogenous fluorophores, tryptophan, NAD(P)H and FAD, present in cells in the UV–VIS spectrum. The excitation and emission band-passes were 2 and 2.5 nm, respectively. The PMT high voltage was set at 950 V, and an integration time of 1 s per wavelength was used in all experiments to achieve an adequate signal-to-noise ratio while minimizing the measurement time. This resulted in a total measurement time of 30 min for each cell suspension. A magnetic stirrer was used to keep the cells in suspension during the course of the 30 min measurement time. The stirring speed was determined by finding the minimum speed at which fluorescence intensity remained constant over time to minimize any potential physical damage to the cells. Right-angle collection was used to measure the fluorescence EEM from each cell suspension in order to minimize the detection of the backscattered excitation light. After each experiment, a repeat fluorescence spectrum was measured at 260 nm excitation and compared with that measured at the beginning of the experiment to establish that the measurement protocol used did not induce photobleaching. The peak intensity at an excitation–emission wavelength of 260–340 nm of the repeat fluorescence spectrum was found to be within 10% of that taken at the beginning of the experiment. In addition, the fluorescence intensity at the excitation–emission maxima in the EEM corresponding to tryptophan, NAD(P)H and FAD was measured once per minute (1 s integration time) for a total of 5 min. The average and standard deviation of the five data points provided the reproducibility of the fluorescence measurements obtained from each cell suspension.

Fluorescence measurements were obtained from the cell suspension as well as the PBS media; the latter was subtracted as background fluorescence. The fluorescence intensity at each wavelength of the emission spectrum (for a particular excitation wavelength) was divided by that measured with a reference photodiode in the excitation monochromator; this correction accounts for the wavelength-dependent variations in the lamp intensity and the wavelength-dependent efficiency of the excitation monochromator. A factory-generated correction factor was also used to correct for the wavelength-dependent efficiency of the optical components in the emission monochromator and the PMT. Finally, the fluorescence intensity at each excitation–emission wavelength pair measured from the cells was divided by the peak fluorescence intensity (excitation–emission: 460–575 nm) of a Rhodamine standard dissolved in water (2.14 μM) to correct for day-to-day variations in the throughput of the instrument.

Data analysis to determine the fluorescence intensity per cell. A linear relationship is expected between fluorescence intensity and cell concentration when turbidity is negligible, and the slope of the linear relationship represents the fluorescence intensity per cell. Thus, the fluorescence intensity at each excitation–emission maximum was plotted as a function of the concentration of cells in suspension. The excitation–emission maxima of tryptophan, NAD(P)H and FAD are 280–340 nm, 340–460 nm and 460–520 nm, respectively. Although, tryptophan was observed to maximally fluoresce at 280–340 nm, fluorescence measurements taken at several of the higher cell concentrations saturated the PMT. Thus, the tryptophan fluorescence measured from the cells was analyzed at an excitation–emission wavelength of 300–340 nm.

A linear range was quantitatively determined by doing a series of linear least squares fits (27), in which data points at the upper range of concentrations were sequentially excluded until the R^2 value was maximized. Because the intercept was expected to pass through the origin, it was fixed at zero for each fit. However, it should be noted that similar results were obtained whether or not the intercept of the fit was fixed at zero. The slope and the standard errors of the slope were calculated using the R software package (27). The slope reflects the fluorescence intensity per cell and enables a direct comparison of the intrinsic fluorescence between cell lines. Because each data point in the plot was obtained from an independent culture, the standard error of the slope reflects the interculture variation in the fluorescence measurement.

Determination of cell sizes. Variations in cell size may affect the amount of fluorescence measured per cell. Therefore, the average size of the cells was determined for each cell line. The cells were imaged using a phase-contrast microscope coupled to a CCD camera. These images were imported into ImageJ (NIH, http://rsb.info.nih.gov/ij). Cell areas were determined using the "adjust threshold" and "analyze particles" functions. These functions identify areas contained within the cells and thus provide an area of distribution. This was done for approximately 20 cells within an independent culture for each cell type. The microscope was calibrated such that cell sizes could be reported in absolute units.

Two-photon fluorescence microscopy. The NAD(P)H fluorescence in monolayers of MCF10 pZIP and MCF10 R-Ras cells was imaged using two-photon fluorescence microscopy. These experiments were carried out to compare the fluorescence measurements obtained from cell monolayers with those obtained from cells in suspension. MCF10 pZIP cells and MCF10 R-Ras cells were plated separately on lysine-coated cover glass bottom petri dishes, immersed in their standard growth media and allowed to grow overnight under the same conditions as in the previous experiment (see Preparation of Cell Suspensions). Three pairs of MCF10 pZIP and MCF10 R-Ras cultures were imaged using two-photon fluorescence microscopy. Both cell lines within each pair were imaged under identical experimental conditions.

The two-photon excitation source was a Ti:Sapphire laser tuned to either 775 nm or 789 nm (this difference was due to day-to-day variations in the stability of the laser). The excitation light was delivered to and the emitted light was collected from the sample through a conventional inverted Nikon eclipse microscope (with a 40× oil immersion objective with a numerical aperture of 1.3) coupled to a Biorad confocal scan head. A PMT was used as the detector. The absolute light intensity reaching the sample was approximately 15 mW. The imaging chamber was heated to maintain the cells at 37°C. A series of fluorescence images were obtained as a function of depth (in 0.5 μm increments) such that the image with the largest cross-sectional area per cell could be selected for analysis. At each depth increment, the cells were scanned over an approximately 200×200 μm area such that several cells could be imaged at once. The frame rate was approximately 1 s/slice. The fluorescence images of the cells were background subtracted, *i.e.* by subtracting the intensity observed in a region of the same sample where no cells were present.

Viability after each imaging experiment was verified by checking the imaged cells for normal growth the next day. The viability of the imaged

Table 1. Cell viability data compiled by cell type, collected before and after each fluorescence experiment for four of the five cell types evaluated in this study. The numbers in parentheses within the first column correspond to the number of independent cultures evaluated for each cell type. The time period between pre- and postexperiment viability measurements was approximately 45 min

Cell line	Viability before experiments (%)	Viability after experiments (%)
MCF10 pZIP (n = 8)	91.9 ± 2.5	87.5 ± 5.3
MCF10 R-Ras (n = 7)	93.3 ± 2.1	84.4 ± 11.3
T47D (n = 7)	85.2 ± 1.7	80.7 ± 4.5
MDA231 (n = 7)	88.0 ± 4.8	85.4 ± 4.7

cells was compared with that of nonimaged cells grown and maintained under identical experimental conditions. The imaged cells appeared to remain viable, with no apparent effects caused by the imaging process. Note that the assessment of viability was not carried out quantitatively because the cells would have had to be detached and counted in a hemacytometer. This procedure would require the mixing of a large number of nonimaged cells with a small number of imaged cells.

RESULTS

Table 1 shows the cell viability data compiled by cell type, collected before and after each fluorescence experiment, for four of the five cell types evaluated in this study. The numbers in parentheses within the first column correspond to the number of independent cultures evaluated for each cell type. The time period between pre- and postexperiment viability measurements was approximately 45 min. The viability of all cell types was greater than 85% before the fluorescence experiment and decreased by less than 10% during the course of the experiment.

Figure 1 shows representative fluorescence EEM for the (1) MCF10 pZIP cells and (2) MCF10 R-Ras cells measured at concentrations of 1.07×10^6 cells/mL and 1.20×10^6 cells/mL, respectively. The plots are shown on a log contour scale, where each contour corresponds to levels of equal fluorescence intensity. Fluorescence peaks "T," "N" and "F" are attributed to tryptophan, NAD(P)H and FAD, respectively. The same three peaks were observed in the EEM of the other cell types. Thus, all subsequent analyses focused on the fluorescence peaks corresponding to these three fluorophores. However, an excitation–emission wavelength pair of 300–340 nm was used to quantify tryptophan fluorescence because the fluorescence intensities at an excitation–emission wavelength pair of 280–340 nm (corresponding to the peak fluorescence of tryptophan) were saturated at some of the higher cell concentrations. An evaluation of the fluorescence emission spectra of tryptophan, NAD(P)H and FAD at excitation maxima of 300, 340 and 460 nm, respectively, indicated that the spectral line shapes of these fluorophores are very similar for all cell types.

Figure 2 displays the fluorescence intensity *vs* cell concentration for MCF10 pZIP and MCF10 R-Ras cells at an excitation–emission maximum of (Fig. 2a,b) 300–340 nm (which corresponds to the fluorescence of tryptophan) and (Fig. 2c,d) 340–450 nm (which corresponds to the fluorescence of NAD(P)H). The standard deviations of the fluorescence intensity and the cell concentration are shown for each data point. A least squares fit over the linear range is shown in each plot.

At MCF10 pZIP cell concentrations less than 2.0×10^6 cells/mL, there is a linear relationship between fluorescence intensity and cell concentration at both excitation–emission wavelength

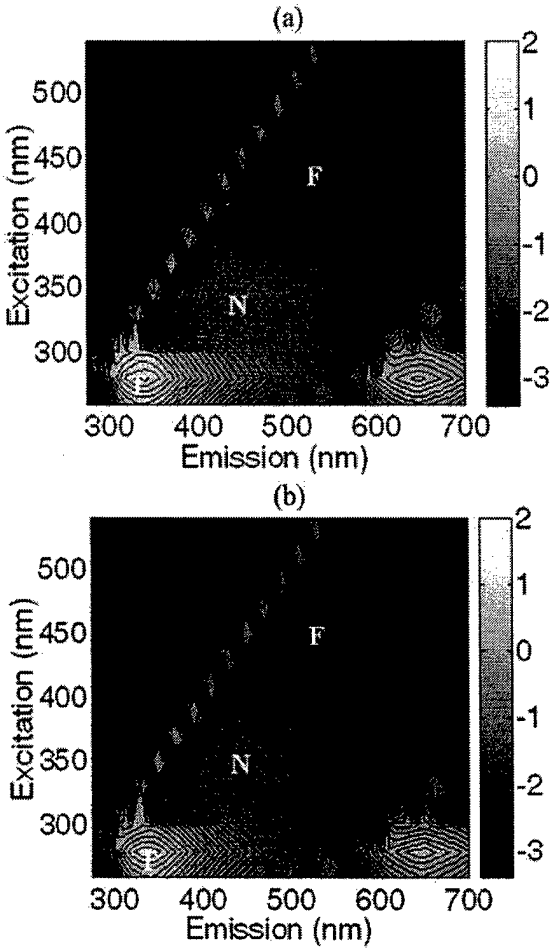

Figure 1. Representative fluorescence EEM for the MCF10 pZIP cells (a) and MCF10 R-Ras cells (b), measured at concentrations of 1.07×10^6 cells/mL and 1.20×10^6 cells/mL, respectively. The plots are shown on a log contour scale, where each contour corresponds to levels of equal fluorescence intensity. Fluorescence peaks "T," "N" and "F" are attributed to tryptophan, NAD(P)H and FAD, respectively.

pairs given (Fig. 2a,c). However, at concentrations that are greater than or equal to 2.0×10^6 cells/mL, the fluorescence intensity saturates with increasing cell concentration at both excitation–emission wavelength pairs given. This is presumably because of the increased turbidity of the cell suspension. On the other hand, the fluorescence intensity of MCF10 R-Ras cells increases linearly with concentration over the entire range up to 3×10^6 cells/mL at both excitation–emission wavelength pairs (Fig. 2b,d).

Table 2 shows the cell concentration at which the linear relationship between the fluorescence intensity and cell concentration saturates for four of the five cell types evaluated in this study. These maximum cell concentration values were found to be the same for fluorescence measurements at the three excitation–emission maxima corresponding to tryptophan, NAD(P)H and FAD. The normal MCF10 pZIP cell line displays saturation in fluorescence intensity at a lower concentration than that of the three malignant cell types.

Figure 3 shows the slope and the standard error for four of the five cell types evaluated in this study at the three excitation–emission maxima corresponding to the fluorescence of tryptophan,

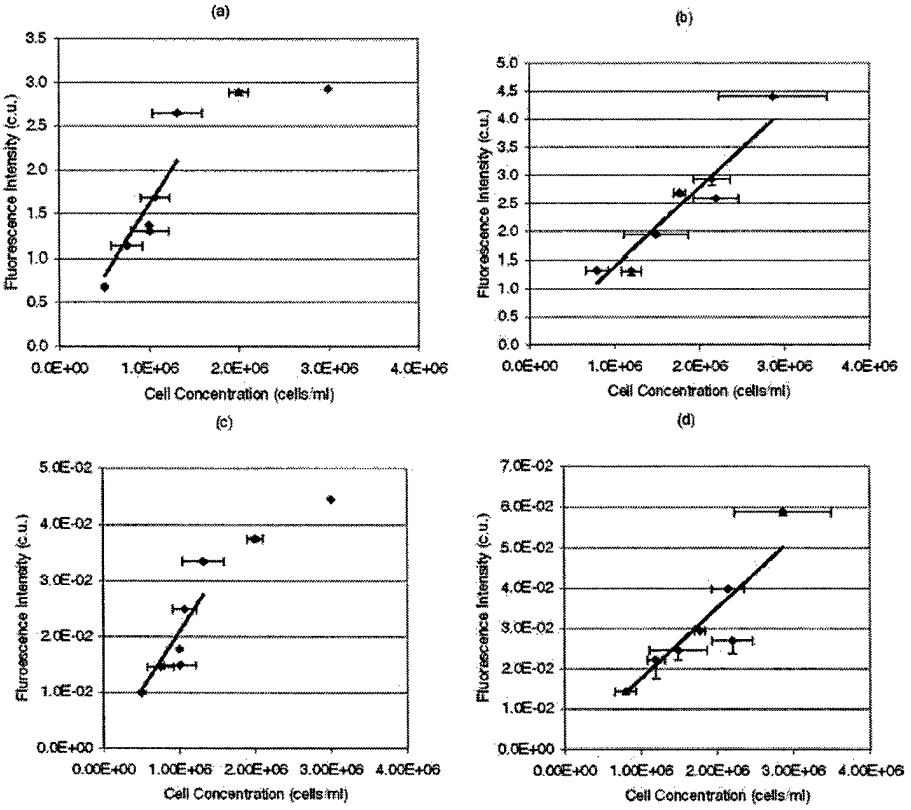

Figure 2. Fluorescence intensity *vs* cell concentration for MCF10 pZIP and MCF10 R-Ras cells at an excitation–emission maximum of 300–340 nm (which corresponds to the fluorescence of tryptophan) (a and b, respectively) and 340–450 nm (which corresponds to the fluorescence of NAD(P)H) (c and d, respectively). The standard deviations of the fluorescence intensity and cell concentration are shown for each data point. A least squares fit over the linear range is shown in each plot.

NAD(P)H and FAD. The slope corresponds to the fluorescence intensity per cell. The slopes are multiplied by a scaling factor to display the fluorescence per cell of the three fluorophores on the same graph (shown in legend).

General linear hypothesis testing (28) was used to determine the level of significance at which differences in tryptophan, NAD(P)H and FAD fluorescence are observed between the normal and malignant cells. All the malignant cells showed a statistically significant decrease in the tryptophan fluorescence per cell relative to that of the normal MCF10 pZIP cells, at a level of significance of $P < 0.002$. No statistically significant differences were observed in the NAD(P)H fluorescence per cell between the normal MCF10 pZIP cells and any of the malignant cell types. The FAD fluorescence per cell of the MCF10 R-Ras cells was increased relative to that of the MCF10 pZIP cells at a level of significance of $P < 0.05$. However, no statistically significant differences were observed in the FAD fluorescence per cell between the normal MCF10 pZIP cells and any of the genetically dissimilar malignant cell types.

As mentioned earlier in Materials and Methods, the fluorescence intensity *vs* cell concentration was also measured from the malignant T47D cells transfected with the R-Ras oncogene. In this case, tryptophan and NAD(P)H fluorescence per cell was not significantly altered, but a statistically significant increase in FAD fluorescence was observed in the T47D R-Ras cells relative to that in the T47D cells. These findings indicate that the decrease in tryptophan fluorescence observed with transformation is not attributed to the expression of the R-Ras oncogene alone but rather to the transformation of the cell from a normal to a malignant phenotype. However, the increase in FAD fluorescence in the MCF10 R-Ras cells, relative to that in the MCF10 pZIP cells, may be because of the transfection of the R-Ras oncogene rather than due to transformation from a normal to a malignant phenotype.

Figure 4 shows the average cell cross-sectional areas (determined from approximately 20 cells for each cell type) for four of the five cell types evaluated in this study. It can be seen that all of the cell types are similar in size, with cell sizes ranging from 150 to 200 μm^2. The variability in size within a cell type appears to be typical of these cells. Figure 4 indicates that the differences in fluorescence intensity per cell between the normal and malignant cells are not attributed to differences in cell size.

Finally, NAD(P)H fluorescence obtained from cells in suspension were compared with that obtained from cell monolayers imaged using two-photon fluorescence microscopy. Figure 5 shows representative fluorescence images of (1) MCF10 pZIP and (2) MCF10 R-Ras cell monolayers at 775 nm excitation (corresponds to single-photon excitation of 387.5 nm), imaged under identical

Table 2. The cell concentration at which the linear relationship between the fluorescence intensity and the cell concentration saturates for four of the five cell types evaluated in this study. These cell concentration values were found to be the same for fluorescence measurements at the three excitation–emission maxima corresponding to tryptophan, NAD(P)H and FAD

Cell line	Cell concentration at which fluorescence saturates (cells/mL)
MCF10 pZIP	2.0×10^6
MCF10 R-Ras	$>3 \times 10^6$
T47D	$>3 \times 10^6$
MDA231	$>3 \times 10^6$

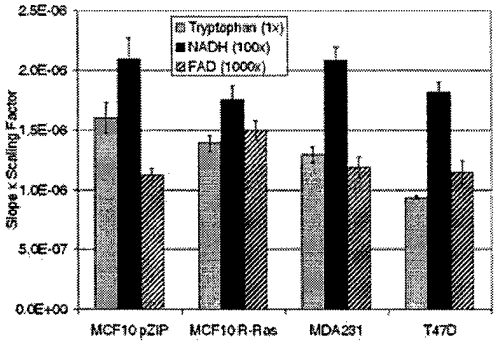

Figure 3. Slope and standard error for four of the five cell types evaluated in this study at the three excitation–emission maxima corresponding to the fluorescence of tryptophan, NAD(P)H and FAD. The slope corresponds to the fluorescence intensity per cell. The slopes are multiplied by a scaling factor to display the fluorescence per cell of the three fluorophores on the same graph (shown in legend).

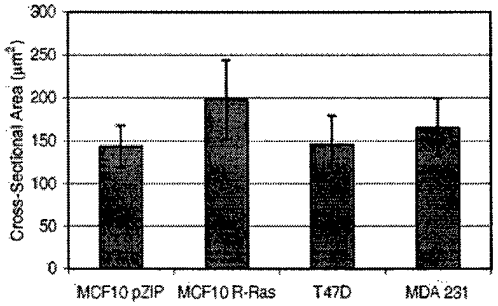

Figure 4. Average cell cross-sectional areas (determined from approximately 20 cells for each cell type) for four of the five cell types evaluated in this study.

experimental conditions. It can be seen that the fluorescence of the MCF10 R-Ras cells is approximately a factor of 2 lower than that of the MCF10 pZIP cells. To evaluate these results quantitatively, ImageJ (NIH, http://rsb.info.nih.gov/ij) was used to (1) manually identify the fluorescence image that displayed the largest cross-sectional area per cell; (2) integrate the fluorescence intensity from each cell; and (3) average the fluorescence intensity from a total of five cells within each monolayer. The ratio of the average fluorescence intensity of the MCF10 pZIP and MCF10 R-Ras cell monolayers (imaged under identical experimental conditions) was then calculated. This ratio was averaged for three independent pairs of MCF10 pZIP and MCF10 R-Ras monolayer images and calculated to be 2.3 ± 1.0. A paired *t*-test (27) was used to determine the level of significance at which differences in NAD(P)H fluorescence are observed between the MCF10 pZIP and MCF10 R-Ras monolayers. The NAD(P)H fluorescence of the MCF10 R-Ras cells was decreased relative to that of the MCF10 pZIP cells at a level of significance of $P < 0.05$. In addition, a qualitative examination of the images showed that there are differences in the spatial distribution of NAD(P)H fluorescence between the MCF10 pZIP and MCF10 R-Ras cells. Specifically, the NAD(P)H fluorescence of the normal MCF10 pZIP cells appeared to be more granular than that of the transformed MCF10 R-Ras cells.

DISCUSSION

The cell suspension studies show that there is a statistically significant decrease in the tryptophan fluorescence per cell in the collective set of malignant cell types compared with that of the normal cell line. However, no statistically significant differences were observed in the NAD(P)H or FAD fluorescence per cell between the normal cells and any of the malignant cell types, based on the cell suspension studies. Two-photon fluorescence microscopy of cell monolayers indicated a statistically significant decrease in the NAD(P)H fluorescence of the MCF10 R-Ras cells relative to that of the MCF10 pZIP cells (normal and malignant cells of similar genetic origins). These results suggest that fluorescence imaging of single cells or the cell monolayer preparation may provide more contrast than volume-averaged fluorescence measurements of cells in suspension. The ultimate goal of this work is to apply these findings to observations in tissue. However, simple cell studies such as the one described here are not directly comparable with tissue studies because a number of other factors are present in tissue, such as the interaction with the extracellular matrix and vasculature. Therefore, it is premature to make any links between the results of our cell studies and previous *ex vivo* studies of the breast.

The differences in the intrinsic fluorescence properties of the normal and malignant cells reflect the amount of fluorophore present or the properties of the surrounding microenvironment (or both) (7). The decreased tryptophan fluorescence observed in the malignant cell lines may indicate that there is a lower protein content in the malignant cells relative to that of the normal cells. In addition, a decreased quantum yield could result from changes in the microenvironment, such as a change in the local prevalence of quenchers such as oxygen.

The results reported for NAD(P)H in our study are inconsistent with that reported by Glassman *et al.* (22), who found that there is an increase in NAD(P)H fluorescence with malignancy. In our cell suspension measurements, no statistically significant differences in the NAD(P)H fluorescence was observed between the normal and any of the malignant cells, whereas in our two-photon fluorescence microscopy study, there was a statistically significant decrease in the NAD(P)H fluorescence of the malignant cells, compared with their genetically similar normal counterpart. The inconsistency between our study and that reported by Glassman *et al.* (22) could be attributed in part to differences in the study design and the sample preparation protocol.

It is instructive to compare the findings from our cell suspension and cell monolayer studies with those that used similar protocols (evaluation of normal and malignant cell lines of genetically similar origins, viability testing and fluorescence measurements at nonturbid cell concentrations). Grossman *et al.* (18) characterized the fluorescence properties of normal and malignant murine fibroblast cell suspensions; the malignant cell line was obtained by transforming the normal cell line with the H-Ras oncogene. They observed a decrease in tryptophan and NAD(P)H fluorescence with malignancy. Their observations relating to tryptophan fluorescence are consistent with that observed in our cell suspension studies, and their findings related to NAD(P)H fluorescence are consistent with that observed in our cell monolayer studies. Pitts *et al.* (5) examined the fluorescence properties of human bronchial epithelial cells, including a normal cell line and a tobacco carcinogen–transformed cell line of the same genetic origin. They found that the NAD(P)H and FAD fluorescence decreased with malignancy but that the tryptophan fluorescence

remained unchanged. Their results for NAD(P)H, which they obtained from cell monolayers, are consistent with those observed in our cell monolayer studies. Their results for FAD and tryptophan are inconsistent with our findings. These inconsistencies may be attributed to the method of transformation of the cells, the cell lines used, the cell preparation method or the measurement technique.

Our results are inconsistent with those reported from a recent study on cervical tissue slices (29), which showed that there is an increase in NAD(P)H fluorescence with neoplasia. The inconsistency between the tissue slice study and our cell study may be explained by the fact that the NAD(P)H fluorescence will be influenced not only by the metabolic demand but also by the oxygen supply available to the cells. The metabolic demand is higher for the proliferative malignant cells compared with their normal counterpart in both cells (30) and tissues (31,32). However, the oxygen supply may be quite different in the two systems. The cellular microenvironment is hyperoxic compared with the tissue microenvironment. Thus, whereas an increase in the metabolic demand may increase NAD(P)H concentration (and fluorescence) in tissues, the reverse may be true in cells, where the oxygen supply is not constrained. As will be discussed below, more complex biological models can be used in the future to evaluate this effect.

The normal MCF10 pZIP cell line showed saturation in fluorescence intensity at concentrations greater than or equal to 2.0×10^6 cells/mL, whereas each of the malignant cell lines showed a linear relationship between fluorescence intensity and cell concentrations up to 3×10^6 cells/mL. The saturation in fluorescence intensity is likely caused by the increased turbidity of the cell suspension. Therefore, these results suggest that the MCF10 pZIP cell suspension is more turbid than the malignant cell suspensions at similar cell concentrations. This may indicate that either the absorption or the scattering properties of normal cells are increased relative to those of the malignant cells. Because saturation of the fluorescence intensity occurs at the same MCF10 pZIP cell concentration at all three excitation–emission maxima, the nonlinearity in fluorescence intensity *vs* concentration is more likely because of scattering (rather than due to absorption). Therefore, it is hypothesized that the MCF10 pZIP cells scatter more than their malignant cell counterpart. There are several studies that support this hypothesis. Croce *et al.* (33) have previously reported that fibroblasts with a malignant phenotype exhibit a decrease in the number of mitochondria and a loss of organization relative to a putatively normal cell line (this may also explain the decreased granularity seen in the mitochondrial NAD(P)H fluorescence in the transformed cells in Fig. 5). Because the mitochondria contribute to a substantial amount of cellular scattering (34), the malignant cells will have decreased scattering relative to their normal counterpart. Zonios *et al.* (35) observed a decrease in the scattering coefficient in adenomatous colon polyps *in vivo*, relative to normal tissues, at wavelengths less than 550 nm. Georgakoudi *et al.* (36) also found that scattering decreased with disease progression in patients with Barrett esophagus.

Backman *et al.* (37) report that there is increased scattering from neoplastic cells relative to nonneoplastic cells and show that this is due to increased scattering from the enlarged nucleus of the neoplastic cells. Their method examined polarized backscattered light, which they report is primarily due to nuclear size (they report that nuclear scattering accounts for the majority of small-angle forward scattering and backscattering, whereas high-angle scattering is due to smaller organelles such as the mitochondria) (37). In our study, the transformed and nontransformed cells had similar nuclear sizes; thus, differences in scattering may be primarily attributed to the differences in the mitochondrial content of malignant and nonmalignant breast cells.

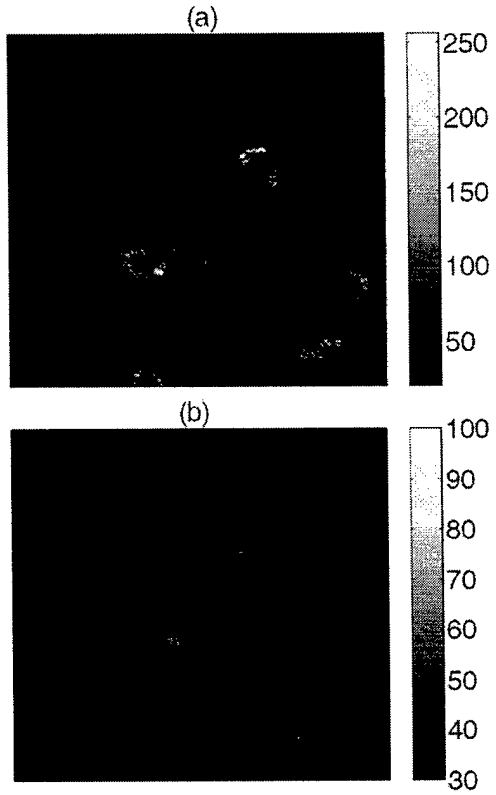

Figure 5. Representative fluorescence image of MCF10 pZIP (a) and MCF10 R-Ras (b) cell monolayers at 775 nm excitation (corresponds to single-photon excitation of 387.5 nm), imaged under identical experimental conditions. Please note the different scales in (a) and (b).

In summary, significant differences have been noted in the fluorescence properties of normal and malignant human breast cells. In future studies it may be possible to build upon these findings in order to understand how the contribution of cellular fluorescence affects fluorescence spectra measured in intact tissue. For example, it is possible to grow epithelial cells in a three-dimensional collagen matrix, thus producing a system in which cell growth and differentiation are modulated by the effects of the extracellular matrix (38). Using such a system, one could potentially examine cellular fluorescence with the added influence of the extracellular matrix on cell growth and differentiation. To more accurately simulate *in situ* conditions, normal and malignant human breast cell lines can be grown subcutaneously in a nude mouse model (39). In such a system the added effects of the vasculature, in addition to the extracellular matrix, on the tissue fluorescence could be studied. A stepwise approach such as this presents the possibility to bridge these studies to fluorescence measurements made on intact human breast tissue.

Acknowledgements—This work was supported by the Whitaker Foundation and the Department of Defense Breast Cancer Research Program. The authors gratefully acknowledge John White, Jayne Squirrell and Kevin Eliceiri for providing assistance with the two-photon microscopy experiments and Jens Eickhoff for assistance in the statistical analysis.

REFERENCES

1. Harris, J. R., M. E. Lippman, M. Morrow and C. K. Osborne (2000) *Diseases of the Breast*. Lippicott Williams & Wilkins, Philadelphia, PA.
2. Ramanujam, N. (2000) Fluorescence spectroscopy of neoplastic and non-neoplastic tissues. *Neoplasia* **2**, 89–117.
3. Brookner, C. K., M. Follen, I. Boiko, J. Galvan, S. Thomsen, A. Malpica, S. Suzuki, R. Lotan and R. Richards-Kortum (2000) Autofluorescence patterns in short-term cultures of normal cervical tissue. *Photochem. Photobiol.* **71**, 730–736.
4. Sokolov, K., J. Galvan, A. Myakov, A. Lacy, R. Lotan and R. Richards-Kortum (2002) Realistic three-dimensional epithelial tissue phantoms for biomedical optics. *J. Biomed. Opt.* **7**, 148–156.
5. Pitts, J. D., R. D. Sloboda, K. H. Dragnev, E. Dmitrovsky and M. A. Mycek (2001) Autofluorescence characteristics of immortalized and carcinogen-transformed human bronchial epithelial cells. *J. Biomed. Opt.* **6**, 31–40.
6. Heintzelman, D. L., R. Lotan and R. R. Richards-Kortum (2000) Characterization of the autofluorescence of polymorphonuclear leukocytes, mononuclear leukocytes and cervical epithelial cancer cells for improved spectroscopic discrimination of inflammation from dysplasia. *Photochem. Photobiol.* **71**, 327–332.
7. Lakowicz, J. R. (1999) *Principles of Fluorescence Spectroscopy*. Kluwer Academic/Plenum, New York.
8. Chance, B., I. A. Salkovitz and A. G. Kovach (1972) Kinetics of mitochondrial flavoprotein and pyridine nucleotide in perfused heart. *Am. J. Physiol.* **223**, 207–218.
9. Thompson, E. W., M. Yu, J. Bueno, L. Jin, S. N. Maiti, F. L. Palao-Marco, H. Pulyaeva, J. W. Tamborlane, R. Tirgari, I. Wapnir *et al.* (1994) Collagen induced MMP-2 activation in human breast cancer. *Breast Cancer Res. Treat.* **31**, 357–370.
10. Ramanujam, N. (2000) Fluorescence spectroscopy in vivo. In *Encyclopedia of Analytical Chemistry* (Edited by R. Meyers), pp. 20–56. John Wiley and Sons, Ltd.
11. Majumder, S. K., P. K. Gupta, B. Jain and A. Uppal (1999) UV excited autofluorescence spectroscopy of human breast tissues for discriminating cancerous tissue from benign tumor and normal tissue. *Lasers Life Sci.* **8**(4), 249–264.
12. Gupta, P. K., S. K. Majumder and A. Uppal (1997) Breast cancer diagnosis using N_2 laser excited autofluorescence spectroscopy. *Lasers Surg. Med.* **21**, 417–422.
13. Yuanlong, Y., E. J. Celmer, M. Zurawska Szczepaniak and R. R. Alfano (1997) Excitation spectrum of malignant and benign breast tissues: a potential optical biopsy approach. *Lasers Life Sci.* **7**, 249–265.
14. Yang, Y., A. Katz, E. J. Celmer, M. Zurawska-Szczepaniak and R. R. Alfano (1997) Fundamental differences of excitation spectrum between malignant and benign breast tissues. *Photochem. Photobiol.* **66**, 518–522.
15. Yang, Y., A. Katz, E. J. Celmer, M. Zurawska Szczepaniak and R. R. Alfano (1996) Optical spectroscopy of benign and malignant breast tissues. *Lasers Life Sci.* **7**, 115–127.
16. Alfano, R. R., A. Pradhan, G. C. Tang and S. J. Wahl (1989) Optical spectroscopic diagnosis of cancer and normal breast tissues. *J. Opt. Soc. Am. B* **6**, 1015–1023.
17. Alfano, R. R., G. C. Tang, A. Pradhan, W. Lam, D. S. J. Choy and E. Opher (1987) Fluorescence spectra from cancerous and normal human breast and lung tissues. *IEEE J. Quantum Electron.* **23**, 1806–1811.
18. Grossman, N., E. Ilovitz, O. Chaims, A. Salman, R. Jagannathan, S. Mark, B. Cohen, J. Gopas and S. Mordechai (2001) Fluorescence spectroscopy for detection of malignancy: H-ras overexpressing fibroblasts as a model. *J. Biochem. Biophys. Methods* **50**, 53–63.
19. Ganesan, S., P. G. Sacks, Y. Yang, A. Katz, M. Al-Rawi, H. E. Savage, S. P. Schantz and R. R. Alfano (1998) Native fluorescence spectroscopy of normal and malignant epithelial cells. *Cancer Biochem. Biophys.* **16**, 365–373.
20. Anidjar, M., O. Cussenot, J. Blais, O. Bourdon, S. Avrillier, D. Ettori, J. M. Villette, J. Fiet, P. Teillac and A. Le Duc (1996) Argon laser induced autofluorescence may distinguish between normal and tumor human urothelial cells: a microspectrofluorimetric study. *J. Urol.* **155**, 1771–1774.
21. Pradhan, A., P. Pal, G. Durocher, L. Villeneuve, A. Balassy, F. Babai, L. Gaboury and L. Blanchard (1995) Steady state and time-resolved fluorescence properties of metastatic and non-metastatic malignant cells from different species. *J. Photochem. Photobiol. B: Biol.* **31**, 101–112.
22. Glassman, W. S., M. Steinberg and R. R. Alfano (1994) Time resolved and steady state fluorescence spectroscopy from normal and malignant cultured human breast cell lines. *Lasers Life Sci.* **6**, 91–98.
23. Keydar, I., L. Chen, S. Karby, F. R. Weiss, J. Delarea, M. Radu, S. Chaitcik and H. J. Brenner (1979) Establishment and characterization of a cell line of human breast carcinoma origin. *Eur. J. Cancer* **15**, 659–670.
24. Cailleau, R., R. Young, M. Olive and W. J. Reeves Jr. (1974) Breast tumor cell lines from pleural effusions. *J. Natl. Cancer Inst.* **53**, 661–674.
25. Soule, H. D., T. M. Maloney, S. R. Wolman, W. D. Peterson Jr., R. Brenz, C. M. McGrath, J. Russo, R. J. Pauley, R. F. Jones and S. C. Brooks (1990) Isolation and characterization of a spontaneously immortalized human breast epithelial cell line, MCF-10. *Cancer Res.* **50**, 6075–6086.
26. Keely, P. J., E. V. Rusyn, A. D. Cox and L. V. Parise (1999) R-Ras signals through specific integrin alpha cytoplasmic domains to promote migration and invasion of breast epithelial cells. *J. Cell Biol.* **145**, 1077–1088.
27. Ihaka, R. and R. Gentleman (1996) R: a language for data analysis and graphics. *J. Comput. Graph. Stat.* **5**, 299–314.
28. Myers, R. H. (1990) *Classical and Modern Regression with Applications*. PWS-KENT, Boston, MA.
29. Drezek, R., C. Brookner, I. Pavlova, I. Boiko, A. Malpica, R. Lotan, M. Follen and R. Richards-Kortum (2001) Autofluorescence microscopy of fresh cervical-tissue sections reveals alterations in tissue biochemistry with dysplasia. *Photochem. Photobiol.* **73**, 636–641.
30. Warburg, O. (1956) On the origin of cancer cells. *Science* **123**, 309–314.
31. Avril, N., M. Menzel, J. Dose, M. Schelling, W. Weber, F. Janicke, W. Nathrath and M. Schwaiger (2001) Glucose metabolism of breast cancer assessed by 18F-FDG PET: histologic and immunohistochemical tissue analysis. *J. Nucl. Med.* **42**, 9–16.
32. Nieweg, O. E., W. H. Wong, S. E. Singletary, G. N. Hortobagyi and E. E. Kim (1993) Positron emission tomography of glucose metabolism in breast cancer. Potential for tumor detection, staging, and evaluation of chemotherapy. *Ann. N. Y. Acad. Sci.* **698**, 423–428.
33. Croce, A. C., A. Spano, D. Locatelli, S. Barni, L. Sciola and G. Bottiroli (1999) Dependence of fibroblast autofluorescence properties on normal and transformed conditions. Role of the metabolic activity. *Photochem. Photobiol.* **69**, 364–374.
34. Mourant, J. R., M. Canpolat, C. Brocker, O. Esponda-Ramos, T. M. Johnson, A. Matanock, K. Stetter and J. P. Freyer (2000) Light scattering from cells: the contribution of the nucleus and the effects of proliferative status. *J. Biomed. Opt.* **5**, 131–137.
35. Zonios, G., L. T. Perelman, V. Backman, R. Manoharan, M. Fitzmaurice, J. Van-Dam and M. S. Feld (1999) Diffuse reflectance spectroscopy of human adenomatous colon polyps in vivo. *Appl. Opt.* **38**, 6628–6637.
36. Georgakoudi, I., B. C. Jacobson, J. Van Dam, V. Backman, M. B. Wallace, M. G. Muller, Q. Zhang, K. Badizadegan, D. Sun, G. A. Thomas, L. T. Perelman and M. S. Feld (2001) Fluorescence, reflectance, and light-scattering spectroscopy for evaluating dysplasia in patients with Barrett's esophagus. *Gastroenterology* **120**, 1620–1629.
37. Backman, V., R. Gurjar, K. Badizadegan, I. Itzkan, R. R. Dasari, L. T. Perelman and M. S. Feld (1999) Polarized light scattering spectroscopy for quantitative measurement of epithelial cellular structures in situ. *IEEE J. Sel. Top. Quantum Electron.* **5**, 1019–1026.
38. Keely, P. J., A. M. Fong, M. M. Zutter and S. A. Santoro (1995) Alteration of collagen-dependent adhesion, motility, and morphogenesis by the expression of antisense alpha 2 integrin mRNA in mammary cells. *J. Cell Sci.* **108**(Pt 2), 595–607.
39. Price, J. E. and R. D. Zhang (1990) Studies of human breast cancer metastasis using nude mice. *Cancer Metastasis Rev.* **8**, 285–297.

Comparison of Multiexcitation Fluorescence and Diffuse Reflectance Spectroscopy for the Diagnosis of Breast Cancer (March 2003)

Gregory M. Palmer*, Changfang Zhu, Tara M. Breslin, Fushen Xu, Kennedy W. Gilchrist, and Nirmala Ramanujam

Abstract—**Nonmalignant ($n = 36$) and malignant ($n = 20$) tissue samples were obtained from breast cancer and breast reduction surgeries. These tissues were characterized using multiple excitation wavelength fluorescence spectroscopy and diffuse reflectance spectroscopy in the ultraviolet-visible wavelength range, immediately after excision. Spectra were then analyzed using principal component analysis (PCA) as a data reduction technique. PCA was performed on each fluorescence spectrum, as well as on the diffuse reflectance spectrum individually, to establish a set of principal components for each spectrum. A Wilcoxon rank-sum test was used to determine which principal components show statistically significant differences between malignant and nonmalignant tissues. Finally, a support vector machine (SVM) algorithm was utilized to classify the samples based on the diagnostically useful principal components. Cross-validation of this nonparametric algorithm was carried out to determine its classification accuracy in an unbiased manner. Multiexcitation fluorescence spectroscopy was successful in discriminating malignant and nonmalignant tissues, with a sensitivity and specificity of 70% and 92%, respectively. The sensitivity (30%) and specificity (78%) of diffuse reflectance spectroscopy alone was significantly lower. Combining fluorescence and diffuse reflectance spectra did not improve the classification accuracy of an algorithm based on fluorescence spectra alone. The fluorescence excitation-emission wavelengths identified as being diagnostic from the PCA-SVM algorithm suggest that the important fluorophores for breast cancer diagnosis are most likely tryptophan, NAD(P)H and flavoproteins.**

Index Terms—**Breast cancer, fluorescence, reflectance, spectroscopy.**

I. Introduction

BREAST cancer screening relies on mammography and clinical breast exam for identifying suspicious lesions. Mammograms are useful in detecting small tumors that may be unnoticeable by physical exam; however, they produce a significant percentage of false positives [1]. As a result, follow up diagnostic procedures such as percutaneous needle biopsy are performed to further evaluate breast abnormalities [1]. Needle biopsy has a limited sampling accuracy because only a few small pieces of tissue are extracted from random locations in the suspicious mass. In some cases, sampling of the suspicious mass may be missed altogether. Consequences include a false-negative rate of 1%–7% [2] when verified with follow up mammography, as well as the requirement of repeat biopsies (percutaneous or surgical) in 9%–18% of patients [3], [4] (due to discordance between histological findings and mammography).

Optical sensors based on ultraviolet-visible (UV-VIS) spectroscopy have the potential to improve the sampling accuracy of core needle biopsy by enabling sampling of multiple tissue sites without the need for biopsy, and by providing real-time diagnosis. Fluorescence and diffuse reflectance spectroscopic measurements in the UV-VIS have been shown to have consistently high sensitivities and specificities for detecting human pre-cancers and cancers, *in vivo* in a number of organ sites including the gastrointestinal tract, bronchus, and cervix [5]. Additionally, several groups have demonstrated that there are significant differences in the fluorescence and diffuse reflectance spectra of normal, benign and malignant breast tissues [6]–[16]. Incorporating UV-VIS spectroscopy as an adjunct diagnostic modality to core needle biopsy could potentially reduce the false negative rate of current needle biopsy procedures. This in turn could potentially lead to fewer repeat biopsies in patients with suspicious breast lesions.

The endogenous fluorophores present in breast tissue include tryptophan, reduced nicotinamide adenine dinucleotide (phosphate) (NAD(P)H), flavin adenine dinucleotide (FAD), and collagen [17]. Tryptophan fluorescence, which has an excitation, emission maximum of 300, 340 nm, is an indicator of protein or free tryptophan content. NAD(P)H and flavoproteins are indicators of metabolic activity [17] and have excitation, emission maxima at 351, 460 nm and 450–520 nm, respectively [17]. Collagen is the primary structural protein in the extracellular matrix. It has several excitation, emission maxima, one of which occurs at 325, 390 nm (due to cross-link fluorescence) [17].

Alfano *et al.* [12] were the first to measure fluorescence spectra of malignant and nonmalignant breast tissues. Since then, several groups have investigated the use of fluorescence spectroscopy for breast cancer detection in *ex vivo* studies [6]–[12]. In the collective set of studies to date, emission spectra were acquired at excitation wavelengths of 300, 340,

Manuscript received November 13, 2002; revised March 1, 2003. This work was supported by the Whitaker Foundation and the U.S. Department of Defense Breast Cancer Research Project. *Asterisk indicates corresponding author.*

*G. M. Palmer is with the Department of Biomedical Engineering at the University of Wisconsin, Madison, WI 53706 USA (e-mail: gmpalmer@wisc.edu).

C. Zhu is with the Department of Electrical and Computer Engineering at the University of Wisconsin, Madison, WI 53706 USA (e-mail: czhu@cae.wisc.edu).

F. Xu is with the Department of Pathology at the University of Wisconsin Medical School, WI 53706 USA (e-mail: fushenxu@hotmail.com).

K. W. Gilchrist is with the Department of Pathology at the University of Wisconsin School of Medicine, WI 53706 USA (e-mail: kwgilchr@facstaff.wisc.edu).

T. M. Breslin is with the Department of Surgery at the University of Wisconsin School of Medicine, WI 53706 USA (e-mail: breslin@surgery.wisc.edu).

N. Ramanujam are with the Department of Biomedical Engineering at the University of Wisconsin, Madison, WI 53706 USA (e-mail: nimmi@engr.wisc.edu).

Digital Object Identifier 10.1109/TBME.2003.818488

458, 488, and 514 nm and excitation spectra were measured at emission wavelengths of 340, 390, and 460 nm from, normal, benign, and malignant breast tissues. Emission spectroscopy measures the fluorescence spectrum, while excitation spectroscopy measures the absorption spectrum of a fluorophore. The wavelength-dependent effects of nonfluorescent absorbers and scatterers in tissue also affect the tissue excitation and emission spectra.

Gupta [7] and Majumder *et al.* [6] analyzed different data sets collected from the same set of breast tissues *ex vivo* and showed that the emission spectra at excitation wavelengths of 340 and 488 nm and excitation spectra at emission wavelengths 390 and 460 nm exhibit significant differences between normal, benign and malignant tissues. Using the integrated emission intensities at an excitation wavelength of 340 nm, in a binary classification scheme, they were able to differentiate malignant from normal and benign tissues with a sensitivity and specificity of 98%. The fluorescence was attributed to reduced nicotinamide adenine dinucleotide (NADH) and collagen. Yang *et al.* [8]–[10] reported that emission spectra at 300-nm excitation and excitation spectra at 340-nm emission (tryptophan is the primary fluorophore) can separate malignant and nonmalignant tissues. They found, for example, that the ratio of normalized intensities at 289 and 268 nm of the excitation spectra discriminate between malignant and fibrous tissues with 93% sensitivity and 95% specificity. Although previous work shows promising results, there are important gaps in these studies that still need to be addressed. The main limitations of previous studies are: 1) fluorescence spectra were obtained only at one or several excitation wavelengths from breast tissues; 2) the utility of combining fluorescence and diffuse reflectance spectroscopy was not evaluated; and 3) the classification accuracy of the diagnostic algorithms were not tested in an unbiased manner.

Spectral differences observed in the fluorescence spectra of normal, benign and malignant breast tissues can also be attributed in part to nonfluorescent absorbers and scatterers. Diffuse reflectance spectroscopy provides a direct measurement of tissue absorption as well as scattering. The primary nonfluorescent absorbers in the UV-VIS in breast tissue are DNA, oxygenated and deoxygenated hemoglobin and β-carotene [18].

Several groups have explored the utility of diffuse reflectance spectroscopy between 250–800 nm, for breast cancer detection *ex vivo* [10], [13]–[15] and *in vivo*[15], [16]. Bigio *et al.* [16] measured diffuse reflectance spectra through a core biopsy needle and during breast cancer surgery and showed that this technique can differentiate malignant from normal tissues with a sensitivity of 60%–70% and a specificity of 85%–95%. The collective set of *ex vivo* and *in vivo* studies [10], [13]–[16] show that diffuse reflectance spectra can differentiate malignant from normal tissues. The changes in the diffuse reflectance of malignant tissues, was attributed to increased DNA, protein and hemoglobin absorption and increased scattering.

The primary goal of the study described here was to characterize the multiexcitation fluorescence spectra (at a total of nine excitation wavelengths in the UV-VIS) and UV-VIS diffuse reflectance spectra of malignant and nonmalignant breast tissues and to identify the optimal spectral features for breast cancer diagnosis. A novel nonparametric algorithm (applicable for small sample sizes) was developed to analyze the breast tissue fluorescence and diffuse reflectance spectra in order to classify a particular sample as malignant or nonmalignant (benign, normal) and a cross-validation scheme was utilized to test the algorithm's classification accuracy in an unbiased manner.

II. Methods

A. Tissue Handling Protocol for Ex Vivo Studies

All of the fluorescence and most of the diffuse reflectance measurements to date have been made on excised breast tissues. However, no systematic investigations have been carried out to assess the effect of excision and time after excision on the tissue fluorescence and diffuse reflectance spectra. Therefore, the effects of tissue handling and storage on optical spectroscopy of excised tissue specimens were systematically evaluated in a previous study [19]. In that study, multiexcitation fluorescence and diffuse reflectance spectra of the epithelial tissue of the hamster cheek pouch was characterized *in vivo*, *ex vivo* (immediately after excision) and after being frozen and thawed. The results indicated that the freezing and thawing process of tissue produces a significant deviation in intensity and line shape relative to the *in vivo* spectra over the entire UV-VIS range. On the other hand, *ex vivo* spectra measured within a short time after excision were found to provide a relatively close approximation of *in vivo* spectra.

B. Optical Spectroscopy of Breast Tissues

Approval for the optical spectroscopy study was obtained from the Institutional Review Board at the University of Wisconsin, Madison. Tissue was obtained from patients undergoing either a lumpectomy, mastectomy or breast reduction surgery. In the routine clinical protocol, tissue specimens were harvested during surgery and normal and tumor tissue samples were cut from the larger specimen. The tissue samples that were cut from the larger specimen were generally at least 1 cm in length/width and 3 mm thick, thus providing a semi-infinite geometry for optical spectroscopy. Optical spectroscopic measurements were carried out on the fresh tissue samples, within two hours after surgical excision. Measurements were made on a total of 56 different tissue samples, from a total of 32 different patients. In the majority of patients who participated in this study, a normal and tumor pair was obtained for optical spectroscopy. When normal and tumor tissue sites were available from a patient, the normal tissue specimen was obtained from the same breast that contained the tumor (bilateral cancer surgeries are relatively rare). In most cases, the normal tissue was obtained as far as possible from the tumor site (generally 1 cm or more from the tumor boundary) in order to minimize the potential effects of malignancy. In a minority of the patients, only either a normal or tumor sample was available for the measurement, usually due to limitations in the size of the surgical specimen.

All measurements were made using a Skinscan spectrofluorometer (JY Horiba, Edison, NJ). This instrument consists of a 150 W xenon lamp, double grating excitation and emission monochromators having fixed bandpasses of 5 nm for both excitation and emission, and a photomultiplier tube (PMT). The adjustable parameters of the system are the wavelength range and increment, the signal acquisition time and the PMT high voltage. The illumination and collection of light was coupled through a fiber optic probe, consisting of a central collection

core with a diameter of 1.52 mm surrounded by an illumination ring, with an outer diameter of 2.18 mm. Both the illumination ring and collection core are made up of 31 individual fibers, each with a core/cladding diameter of 200/245 μm. The numerical aperture of the excitation and emission fibers is 0.22 and 0.12, respectively. The probe geometry was designed to maximize the probing depth in the tissue, while providing good signal-to-noise ratio. Simulations using a modified, three-dimensional, weighted-photon Monte Carlo code have been carried out to evaluate the probing depth achieved with this illumination and collection geometry in a turbid medium [20]. For a homogeneous medium with a fixed scattering coefficient of 110.4 cm^{-1}, and absorption coefficient varying from 31.8 cm^{-1} to 1.3 cm^{-1} (i.e., absorption coefficients spanning the UV-VIS range), the probing depth varied from 450 to 1350 μm. In a turbid medium with a fixed absorption coefficient of 10.8 cm^{-1}, and scattering coefficient varying from 225 cm^{-1} to 50 cm^{-1} (i.e., scattering coefficients spanning the UV-VIS range), the probing depth varied from 550 to 1050 μm. The probing depth in a medium with absorption (2.3 cm^{-1}) and scattering coefficients (167 cm^{-1}) representative of breast adipose tissue at 540 nm [21] was 1050 μm.

Fluorescence emission spectra were recorded at excitation wavelengths of 300 to 460 nm, in 20-nm increments. At each excitation wavelength, fluorescence emission was recorded from 10 nm greater than the excitation wavelength, up to 600 nm, in 5-nm increments (e.g., 310 to 600 nm at an excitation wavelength of 300 nm). Fluorescence emission spectra were obtained at a total of nine excitation wavelengths. A signal acquisition time of 0.5 s was used per excitation-emission wavelength pair and the PMT high voltage was set at 950 V for all measurements. The total measurement time was approximately 8 min. The fluorescence emission spectral intensities at each excitation wavelength were normalized to that of a reference photodiode, which accounts for wavelength-dependent variations of the excitation light intensity. The fluorescence emission spectrum at each excitation wavelength was corrected for wavelength dependencies in the emission monochromator and PMT using instrument specific correction factors. Finally, all fluorescence emission spectral intensities were divided by the peak fluorescence intensity (excitation-emission: 460–575 nm) of a Rhodamine B dye (115H3423, Sigma Chemical Co., MO) dissolved in water (2.14 μM), measured after each patient study to correct for time-dependent changes in the throughput of the instrument.

Diffuse reflectance was measured from 300 to 600 nm. This measurement was made in a synchronous scan mode, whereby the excitation and emission gratings are moved simultaneously. The diffuse reflectance measurements were made at an increment of 5 nm, with a signal acquisition time of 0.1s/wavelength and at a PMT high voltage of 340 or 450 V. The difference in the PMT high voltage is due to two different instruments being used in the course of the study (both identical models), each having slightly different throughputs. The instruments were otherwise identical and were calibrated, such that this difference does not introduce artifacts into the data. The diffuse reflectance spectrum was corrected for the wavelength-dependent system response and the throughput of the instrument by normalizing it to that of a Spectralon 99% reflectance puck (SRS-99–010, Labsphere, Inc., North Sutton, NH), which was measured with the probe in contact with the puck (no coupling media was used).

TABLE I
HISTOLOGICAL BREAKDOWN OF THE 56 BREAST TISSUE SAMPLES EXAMINED IN THE OPTICAL SPECTROSCOPY STUDY

Total Malignant Tissues	**20**
Invasive ductal carcinoma (IDC)	16
Invasive lobular carcinoma	2
Carcinoma in situ (CIS)	1
CIS + IDC combined	1
Total Normal/Benign Fibrous Tissues	**15**
Normal fibrous tissue	8
Adenosis	2
Reparative Changes	2
Fibrocystic disease	1
Fibroadenoma	1
Cystic	1
Total Normal Adipose Tissues	**21**

After each measurement, the exact site where the probe was positioned on each tissue sample was inked (TMD-BK, Triangle Biomedical Sciences, Durham, NC) and then cut and stained for histopathology. Microscopic evaluation of each histological section was performed (KG, FX) and a consensus diagnosis was reached. When a sample exhibited a heterogeneous diagnosis at the site of measurement, the most severe diagnosis was used (e.g., for samples which had both normal glandular tissue as well as malignant tissue, the sample diagnosis was designated as being malignant). In samples in which both normal adipose and fibroglandular tissues were present, the histology was designated to be that of the predominant tissue type at the site of measurement. Table I shows the histological breakdown of the 56 breast tissue samples examined in the optical spectroscopy study. Eleven of the malignant samples had a histological normal counterpart from the same patient.

C. Data Analysis

Fig. 1 shows the flow chart of the algorithm that was developed to analyze breast tissue fluorescence and diffuse reflectance spectra. Two different types of input data sets were used. In the first case, the original spectra were used. The primary sources of variance in the original spectra are the intensity and spectral line shape. In the second case, each fluorescence spectrum was normalized to its peak intensity, or in the case of the diffuse reflectance spectrum, to its integrated intensity. The primary source of variance in this case was attributed to the spectral line shape. The benefit of preprocessing by normalization is that it cancels out inter-patient variations in intensity and allows a direct comparison of spectral line shape.

Principal Component Analysis (PCA) was employed as a data reduction technique [22]. PCA characterizes a majority of the variance while greatly reducing the input data set into a few orthogonal variables. The principal components (PCs) are extracted such that the first principal component (PC1) accounts for the largest amount of the total variance of the input data. The second PC (PC2) accounts for the second largest amount of the variance while being orthogonal to PC1, and so on. Thereby PCA projects the set of observed data onto a subspace expanded by the PCs. There are two advantages of this transformation: 1) the input data can be represented by a few subsets of PCs with

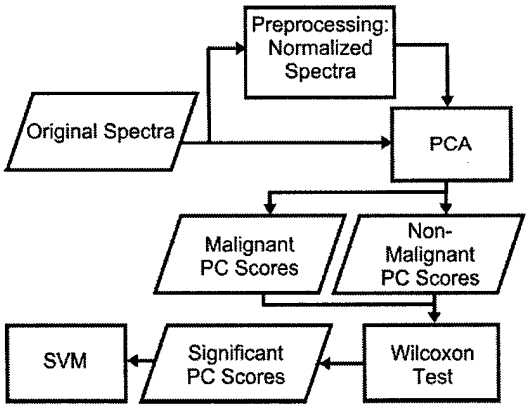

Fig. 1. Flow chart of the algorithm that was developed to analyze breast tissue fluorescence and diffuse reflectance spectra (PCA—principal component analysis; SVM—support vector machine).

minimal mean square error, which reduces the dimensionality of the data set; 2) the projection onto the PC subspace maximizes the separation of data clusters. PCA can be carried out on concatenated spectra (fluorescence emission spectra at all nine excitation wavelengths and diffuse reflectance spectra). Alternatively, PCA can be performed on all fluorescence emission spectra, one excitation wavelength at a time and individually on the diffuse reflectance spectra. Both approaches will yield the same set of eigenvectors for each spectrum. However, in the first case, one set of PC scores will be generated for all spectra per sample, whereas in the second case, one set of PCs will be generated for each spectrum per sample. In this study, PCA was performed on all fluorescence emission spectra, one excitation wavelength at a time and separately on the diffuse reflectance spectra to yield a set of PCs for each spectral data set. The subsets of PCs that account for the majority (95% or 99%) of the variance, rather than all of the PCs, were retained for further processing. Using more PCs (99% versus the 95% criterion) retains a greater proportion of the variance of the input data set.

A Wilcoxon rank-sum (unpaired) or rank-signed (paired) test [23] was then employed to determine which PC scores showed statistically significant differences between malignant and nonmalignant tissue types. This particular test was used because it is a nonparametric test, which is appropriate for small sample sizes for which a normal distribution cannot be assumed. Using a standard criterion of $p < 0.05$, PCs from all nine fluorescence spectra and the diffuse reflectance spectrum showed significant differences between malignant and nonmalignant tissues. However, in a clinical setting, it would be desirable to limit the number of measurement parameters (and thus the measurement time) required for diagnosis. Thus, PCs that showed differences between malignant and nonmalignant tissue types at varying significance levels of $p < 0.05$, $p < 0.005$ and $p < 0.0005$ were retained as inputs into the classification scheme. This was carried out to evaluate the classification accuracy as a function of the number of PCs (or measurement parameters) retained.

A support vector machine (SVM) algorithm [24] was used as the classification technique. SVM is a classification algorithm based on statistical learning theory. The principal idea of an SVM is to determine an optimal separating hyperplane that maximizes the margin between two classes in a multidimensional data space. With the largest separation of the two data clusters, the SVM classifier gives a lower expected risk, which means that future error can be minimized if more data is added to the sample pool. Specifically, a linear kernel SVM classifier was employed in this study, and the classification was carried out on PCs retained from both fluorescence spectra and the diffuse reflectance spectrum or the diffuse reflectance spectrum only.

A full cross-validation of the algorithm was performed in the following manner. First, one sample was removed from the training dataset. The spectra of the remaining samples underwent the steps of preprocessing, PCA, Wilcoxon testing and SVM classification. The optimal PC scores (and corresponding eigenvectors) were identified from the Wilcoxon test and the optimal decision hyperplane was determined from the SVM analysis. Next, the optimized algorithm was applied to the sample that had been left out. In particular, the PC scores were calculated from the sample spectra using the optimal eigenvectors retained from the training set. Then, the sample was classified as malignant or nonmalignant based on which side of the optimal decision hyperplane its PC scores were distributed. This method allowed for an unbiased evaluation of the algorithm's performance when the sample size is too small to separate into independent training and testing data sets. This procedure was carried out for all of the 56 samples. For each testing sample, the algorithm was trained on the remaining 55 training samples.

In the original stages of algorithm development, a two-step algorithm was employed to differentiate between malignant and nonmalignant (normal and benign) tissues. This involved first discriminating between fibrous/glandular and adipose tissues and then discriminating between malignant and fibrous/glandular tissues. This step-wise approach resulted in samples being misclassified at each step. It was observed that a greater number of samples were misclassified using this approach relative to that in which the algorithm was used to directly discriminate between the two classes of interest i.e., malignant and nonmalignant (normal and benign) tissue. Therefore, the latter approach was employed in this study.

It is desirable to relate the PCs that contribute to optimal classification of malignant and nonmalignant breast tissues to features in the corresponding spectrum. This can be achieved by re-projecting the PCs back into the spectral data space. Re-projection of the PC of a given sample into the spectral data space can be achieved by multiplying the PC score of that sample by the corresponding eigenvector. A linear combination of the re-projected PCs that account for 100% of the variance can faithfully reconstruct the spectrum of that sample. Since the objective is to determine which spectral features are useful in the classification, only those PCs that showed the statistically most significant differences between malignant and nonmalignant tissues were used in the re-projection.

III. Results

Fig. 2 shows the average fluorescence excitation-emission matrices (EEMs) for malignant (20) [Fig. 2(a)], normal/benign fibrous (15) [Fig. 2(b)], and adipose tissues (21) [Fig. 2(c)]. Each EEM is shown on a log contour scale, where each contour corresponds to levels of equal fluorescence intensity. The useful fluorescence information is to the right of the Rayleigh scattering line seen in the upper left quadrant of the plot. This

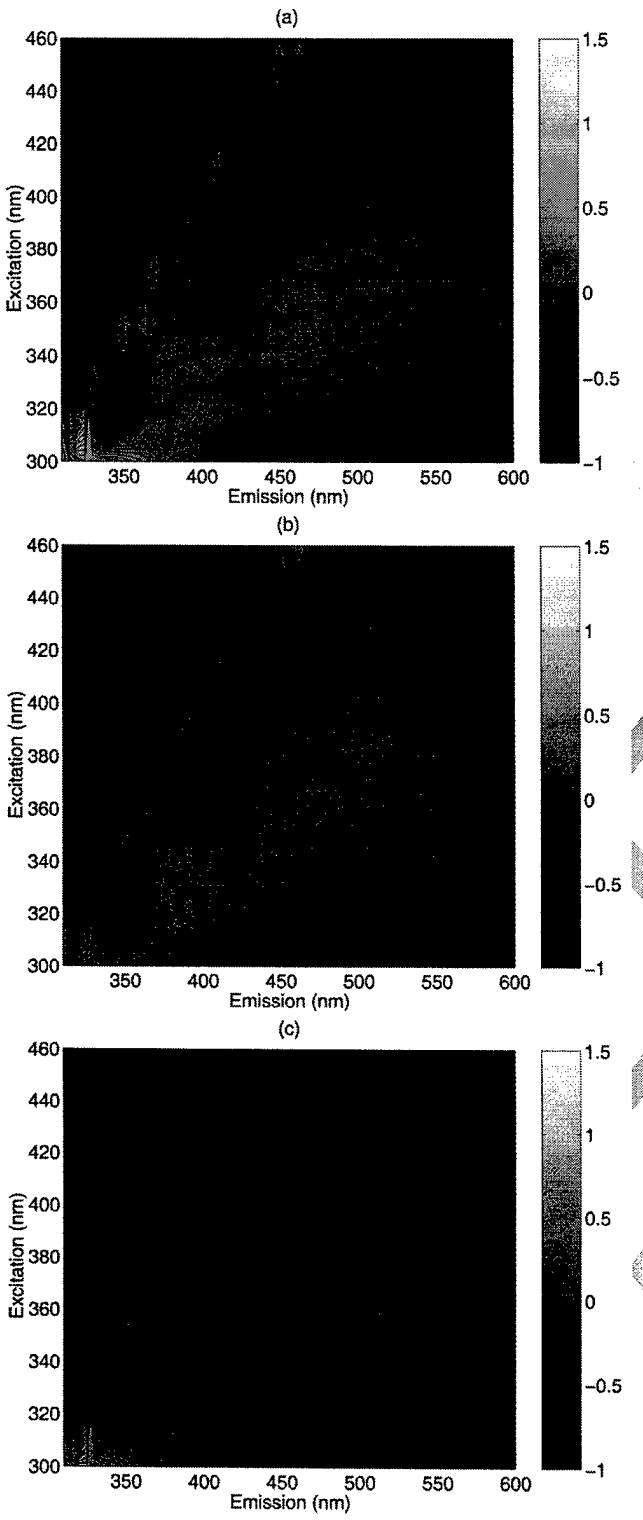

Fig. 2. Average fluorescence EEMs for (a) malignant ($n = 20$), (b) normal/benign fibrous ($n = 15$), and (c) adipose tissues ($n = 21$). Each EEM is shown on a log contour scale, where each contour corresponds to levels of equal fluorescence intensity. The useful fluorescence information is to the right of the Rayleigh scattering line seen in the upper left quadrant of the plot.

plot allows for the display of fluorescence intensities acquired at multiple excitation wavelengths where, the fluorescence spectrum at each excitation wavelength is corresponds to a horizontal slice through the plot. Four peaks are visible in the malignant [Fig. 2(a)] and normal/benign fibrous tissues [Fig. 2(b)], which occur in similar locations, i.e., at excitation, emission wavelength pairs of (300, 340), (340, 390), (360, 460), and (440, 520) nm. The adipose tissue EEM [Fig. 2(c)] on the other hand, shows distinct differences, relative to that observed in Fig. 2(a) and (b). Notably, the peak at (340, 390) nm is weakly present and the peak at (360, 460) nm has been shifted to approximately (360, 520) nm.

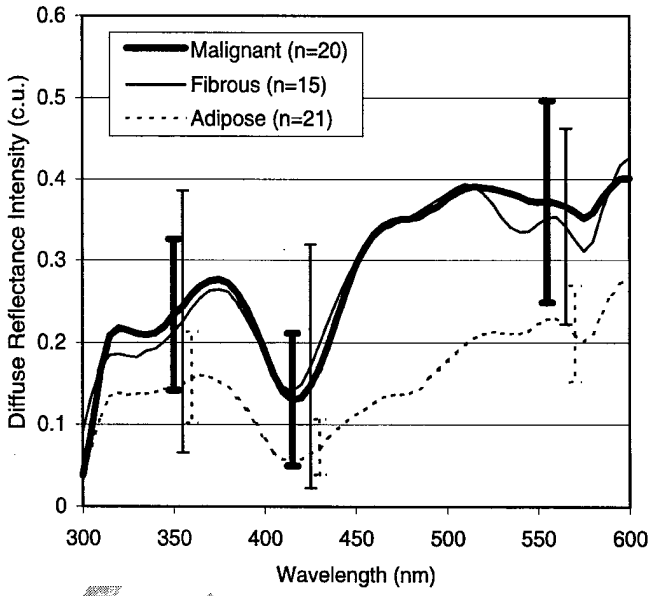

Fig. 3. Average diffuse reflectance spectra with standard deviations, for the malignant, normal/benign fibrous and adipose tissues.

Fig. 3 shows the average diffuse reflectance spectra with standard deviations for the malignant, normal/benign fibrous and adipose tissues. It can be seen that the average malignant and normal/benign fibrous tissue spectra have similar intensities, but subtle differences in spectral line shape in the wavelength regions between 300–350, 400–450 and 525–575 nm. The average adipose tissue spectrum shows decreased intensity at all wavelengths, and a distinctly different line shape between 425–525 nm compared to the average malignant and normal/benign fibrous tissue spectra. Note also that the variability in adipose tissue spectra is significantly less than that of fibrous and malignant tissues.

Table II shows the results of PCA, followed by a Wilcoxon rank-sum test for original [Table II(a)] and normalized [Table II(b)], fluorescence and diffuse reflectance spectra. The PCs that display differences between the malignant and nonmalignant tissues at different significance levels are listed. Each table is arranged to show which PCs meet a particular criterion but do not meet a higher criterion [for example in Table II(b), PC2 at 320-nm excitation meets both the $p < 0.05$ and $p < 0.005$ criterion but not $p < 0.0005$ criterion, and so is shown in the $p < 0.005$ column]. The PCs are organized based on which spectra they were derived from. For a particular spectrum, the PC number and the variance described by that PC (in parentheses) are indicated. Note that Table II shows the results of PCA and the Wilcoxon rank-sum test for all 56 samples.

TABLE II
THE RESULTS OF PCA, FOLLOWED BY A TWO-TAILED WILCOXON RANK-SUM TEST FOR (A) ORIGINAL AND (B) NORMALIZED FLUORESCENCE AND DIFFUSE REFLECTANCE SPECTRA. THE PCS THAT DISPLAY DIFFERENCES BETWEEN THE MALIGNANT AND NONMALIGNANT TISSUES AT DIFFERENT SIGNIFICANCE LEVELS ARE LISTED. EACH TABLE IS ARRANGED TO SHOW WHICH PCS MEET A PARTICULAR CRITERION BUT DO NOT MEET A HIGHER CRITERION (FOR EXAMPLE IN (B), PC2 AT 320 NM EXCITATION MEETS BOTH THE $p < 0.05$ AND $p < 0.005$ CRITERION BUT NOT $p < 0.0005$ CRITERION, AND SO IS SHOWN IN THE $p < 0.005$ COLUMN). THE PCS ARE ORGANIZED BASED ON WHICH SPECTRA THEY WERE DERIVED FROM. FOR A PARTICULAR SPECTRUM, THE PC NUMBER AND THE VARIANCE DESCRIBED BY THAT PC (IN PARENTHESES) ARE INDICATED. NOTE THAT TABLE II SHOWS THE RESULTS OF PCA AND THE WILCOXON RANK-SUM TEST FOR ALL 56 SAMPLES

Spectra	p<0.05	p<0.005	p<0.0005
300 nm Exc.	PC2 (0.06)		PC1 (0.93)
320 nm Exc.	PC1 (0.90)		
340 nm Exc.	PC1 (0.90)		
360 nm Exc.	PC1 ((0.89)		
380 nm Exc.	PC1 (0.97)		
400 nm Exc.	PC1 (0.991)		
420 nm Exc.	PC1 (0.995)		
440 nm Exc.	PC1 (0.996)		
460 nm Exc.	PC1 (0.997)		
Reflectance		PC1 (0.80)	

(a)

Spectra	p<0.05	p<0.005	p<0.0005
300 nm Exc.			PC2 (0.12)
320 nm Exc.	PC1 (0.72)	PC2 (0.17)	
340 nm Exc.	PC1 (0.95)		
360 nm Exc.	PC1 (0.75)		
380 nm Exc.	PC1 (0.77)		
400 nm Exc.		PC1 (0.68)	PC4 (0.02)
420 nm Exc.	PC3 (0.03)		PC1 (0.66)
440 nm Exc.		PC4 (0.02), PC1 (0.67)	
460 nm Exc.			PC3 (0.05)
Reflectance	PC3 (0.12), PC2 (0.37)		

(b)

A comparison of Table II(a) and (b) indicates that far more PCs at higher significance levels ($p < 0.005$ and $p < 0.0005$) are generated using normalized versus the original fluorescence spectra. Thus, this preprocessing method was utilized in all subsequent analysis of fluorescence spectra. It is interesting to note that both the original and normalized fluorescence spectra at 300-nm excitation yield PCs that meet the $p < 0.0005$ criterion. In Table II(b), it can be seen that as the significance level increases, the PCs that are retained from the fluorescence spectral data account for a smaller percent of the total variance. At a significance level of $p < 0.005$, the most useful fluorescence spectra are those measured at 300, 320, 400, 420, 440, and 460 nm excitation. In the case of the diffuse reflectance measurements, the original spectrum [Table II(a)] yields only one PC that meets the $p < 0.005$ criterion, while the normalized spectrum [Table II(b)] yields two PCs that meet the $p < 0.05$ criterion, but not the $p < 0.005$ criterion. Thus, both preprocessing methods were thus utilized in subsequent analysis of diffuse reflectance spectra.

PCs at higher significance levels are generated from fluorescence spectra than from the diffuse reflectance spectra. In Table II(a), there is one PC retained from the fluorescence spectrum at 300 nm, excitation, which is statistically more significant than the PC retained from the diffuse reflectance spectrum. In Table II(b), there are a total of seven PCs retained from fluorescence spectra at several excitation wavelengths that are statistically more significant than the two PCs retained from the diffuse reflectance spectrum.

In addition to the unpaired Wilcoxon rank-sum text, a Wilcoxon rank-signed test of normal/malignant PC pairs within the same patient was performed for a total of 11 normal/malignant tissue pairs. The Wilcoxon rank-signed test resulted in similar PCs to that generated from the Wilcoxon rank-sum test. Specifically, 11 of the 15 PCs identified as being significant from an unpaired analysis of normalized spectra [Table II(b)] were also identified as being significant from a paired analysis of the normalized spectra. The consistency between the paired and unpaired analysis confirms that the observed spectral differences between malignant and nonmalignant tissues are similar within and between patients.

Table III shows the classification results obtained from SVM analysis of the diagnostically important PCs derived from normalized spectra. The PCs used are similar to those indicated in Table II(b). However, it should be noted that Table II shows the results of PCA and the Wilcoxon rank-sum test for all 56 samples, while in the actual algorithm development, only 55 samples were used at a time in the training set (one testing sample was removed sequentially for the purposes of cross-validation). Thus, the PCs shown in Table II could vary slightly from those identified from the 56 independent training sets. The classification rate, sensitivity and specificity for the training and testing data sets are shown for PCs retained at progressively increasing levels of significance ranging from $p < 0.05$ to $p \ll 0.0005$. As seen in Table II(b), the PCs retained at the $p < 0.05$ significance level originate from both the fluorescence and diffuse reflectance spectra, while those retained at higher significance levels originate only from the fluorescence spectra. The PCs in the first three rows were identified from a set of PCs that describe 95% of the variance of the input data set. The PCs in the fourth row were identified from a set of PCs that describe 99% of the variance of the input data set. Increasing the percent variance from 95% to 99% results in two to three more PCs at the $p < 0.0005$ level. The training data set shows a classification accuracy (classification rate, sensitivity and specificity) that corresponds to the average and standard deviation of that obtained from training with a total of 56 data sets, each with a total of 55 samples (one sample at a time of a total of 56 samples was left out for the purposes of cross-validation). The classification accuracy of the testing data set reflects the unbiased performance of the algorithm on 56 samples through cross-validation.

Table III shows that cross-validation of the algorithm results in a 5%–20% decrease in the classification accuracy. It is interesting to note that that the classification accuracy of the testing data set shows a smaller deviation relative to that of the training data set as the number of PCs used in the SVM analysis is reduced (by increasing the level of significance). Furthermore, the classification accuracy of testing data set increases slightly for increasing levels of significance. Selecting the diagnostically relevant PCs at the $p < 0.0005$ level of significance from a set of PCs that describe 99% as opposed to 95% of the variance of the input data set gives rise to an increase in the number of PCs used for SVM classification. This results in an improvement of the overall classification accuracy, as well as the smallest dif-

TABLE III

THE CLASSIFICATION RESULTS OBTAINED FROM SVM ANALYSIS OF THE DIAGNOSTICALLY IMPORTANT PCS DERIVED FROM NORMALIZED SPECTRA. THE CLASSIFICATION RATE, SENSITIVITY AND SPECIFICITY FOR THE TRAINING AND TESTING DATA SETS ARE SHOWN FOR PCS RETAINED AT PROGRESSIVELY INCREASING LEVELS OF SIGNIFICANCE RANGING FROM $p < 0.05$ TO $p < 0.0005$. AS SEEN IN TABLE II(B),THE PCS RETAINED AT THE $p < 0.05$ SIGNIFICANCE LEVEL ORIGINATE FROM BOTH THE FLUORESCENCE AND DIFFUSE REFLECTANCE SPECTRA, WHILE THOSE RETAINED AT HIGHER SIGNIFICANCE LEVELS ORIGINATE ONLY FROM THE FLUORESCENCE SPECTRA. THE PCS IN THE FIRST THREE ROWS WERE IDENTIFIED FROM A SET OF PCS THAT DESCRIBE 95% OF THE VARIANCE OF THE INPUT DATA SET. THE PCS IN THE FOURTH ROW (ASTERISKS) WERE IDENTIFIED FROM A SET OF PCS THAT DESCRIBE 99% OF THE VARIANCE OF THE INPUT DATA SET. THE TRAINING DATA SET SHOWS A CLASSIFICATION ACCURACY (CLASSIFICATION RATE, SENSITIVITY AND SPECIFICITY) THAT CORRESPONDS TO THE AVERAGE AND STANDARD DEVIATION OF THAT OBTAINED FROM TRAINING WITH A TOTAL OF 56 DATA SETS, EACH WITH A TOTAL OF 55 SAMPLES (ONE SAMPLE AT A TIME OF A TOTAL OF 56 SAMPLES WAS LEFT OUT FOR THE PURPOSES OF CROSS-VALIDATION). THE CLASSIFICATION ACCURACY OF THE TESTING DATA SET REFLECTS THE UNBIASED PERFORMANCE OF THE ALGORITHM ON 56 SAMPLES THROUGH CROSS-VALIDATION

Significance Level	Number of PCs	Classification Rate (%)		Sensitivity (%)		Specificity (%)	
		Training Data	Testing Data	Training Data	Testing Data	Training Data	Testing Data
P<0.05	14~15	91.53±2.76	75	84.16±5.66	65	95.60±2.10	80.56
P<0.005	7~8	86.95±1.87	76.79	77.36±4.65	65	92.27±3.06	83.33
P<0.0005	3~4	83.51±1.89	79	76.07±5.61	70	87.63±2.63	83.33
*P<0.0005	6~7	87.56±2.13	83.93	76.35±5.54	70	93.78±1.92	91.67

TABLE IV

CLASSIFICATION RESULTS OBTAINED FROM SVM ANALYSIS OF THE DIAGNOSTICALLY IMPORTANT PCS DERIVED FROM BOTH THE ORIGINAL AND NORMALIZED DIFFUSE REFLECTANCE SPECTRA. THIS A SIMILAR FORMAT TO TABLE III

Pre-processing	Significance Level	Number of PCs	Classification Rate (%)		Sensitivity (%)		Specificity (%)	
			Training Data	Testing Data	Training Data	Testing Data	Training Data	Testing Data
Original	P<0.1	2	66.62±2.51	60.71	45.43±8.85	30	78.38±1.73	77.78
Normalized	P<0.05	2	69.46±5.72	50	51.38±16.3	20	79.41±5.07	66.67

ference in the classification accuracy (in particular, the specificity) between the training and testing data sets. A comparison of the classification accuracy of PCs retained at the $p < 0.0005$ and $p < 0.05$ level of significance in Table III indicates that combining the normalized fluorescence and diffuse reflectance spectra does not improve the classification accuracy of an algorithm based on normalized fluorescence spectra alone.

Table IV shows classification results obtained from SVM analysis of the diagnostically important PCs derived from both the original and normalized diffuse reflectance spectra. This table has a similar format to Table III. Again the PCs selected for this analysis are similar to those shown in Table II. Table II shows that only one PC was retained from the original diffuse reflectance spectra [Table II(a)] and two PCs were retained from the normalized diffuse reflectance spectra [Table II(b)] when a criterion of $p < 0.05$ was used. In order to carry out SVM analysis, at least two features (PCs) are needed. Thus, the $p < 0.1$ criterion was used in order to select at least two diagnostically relevant PCs from the original diffuse reflectance spectra.

Table IV shows that cross-validation of the algorithm results in a 10%–30% decrease in the classification accuracy. The classification accuracy of the testing data set shows a smaller deviation relative to that of the training data set for PCs derived from the original diffuse reflectance spectra. In addition, the classification accuracy of testing data set for PCs extracted from the original spectra is higher than that for PCs derived from the normalized spectra. A comparison of the classification accuracy of PCs retained at the $p < 0.05$ or $p < 0.1$ level of significance in Table IV and $p < 0.0005$ level of significance in Table III indicates that using normalized fluorescence spectra yields significantly higher classification accuracy than using either the original or normalized diffuse reflectance spectra alone.

Fig. 4 shows the average normalized fluorescence spectra at 300-nm excitation [Fig. 4(a)] and the average spectral representations reflected by PC2 (which was obtained from the normalized fluorescence spectra at 300 nm, excitation), for malignant and nonmalignant tissues, and the difference spectra (between malignant and nonmalignant tissues) for each case [Fig. 4(b)]. The spectral representations are re-projections from the PC subspace onto the normalized spectral data space. They are calculated by simply multiplying the PC scores (in this case, PC2) for all samples by the associated eigenvector and then averaging the spectral representations for each tissue type (malignant and nonmalignant). The difference spectrum was obtained by subtracting (point-by-point) the average nonmalignant spectrum from the average malignant spectrum. PC2 was selected for the spectral representation because the Wilcoxon rank-sum test indicated that PC2 displays the statistically most significant differences between malignant and nonmalignant tissues. It should be pointed out that although PC1 accounts for more of the variance in the spectral data than PC2, it also reflects the variance present in both malignant and nonmalignant tissues.

In Fig. 4(a), the average normalized fluorescence spectrum of the malignant tissues shows a red shift in the fluorescence peak and a lower intensity between 450–550 nm relative to nonmalignant tissues. These differences are reflected in the average spectral representation of the malignant and nonmalignant tissues. The differences seen in the average malignant and nonmalignant tissue spectral representations track the differences observed in their corresponding average normalized fluorescence spectra, but do not necessarily replicate the actual spectra itself, since only one PC is used in the re-projection. Fig. 4(b) shows the difference spectra (between malignant and nonmalignant tissues) for both the average normalized spectra and average spectral representations shown in Fig. 4(a). It can be seen that the two difference spectra are very similar to each other, as expected. This verifies that the PC2 displays the most significant difference between the two tissue types. The difference spectra indicate that the most significant differences between malignant and nonmalignant tissues are observed near emission wavelengths of 350 and 500 nm, when an excitation wavelength

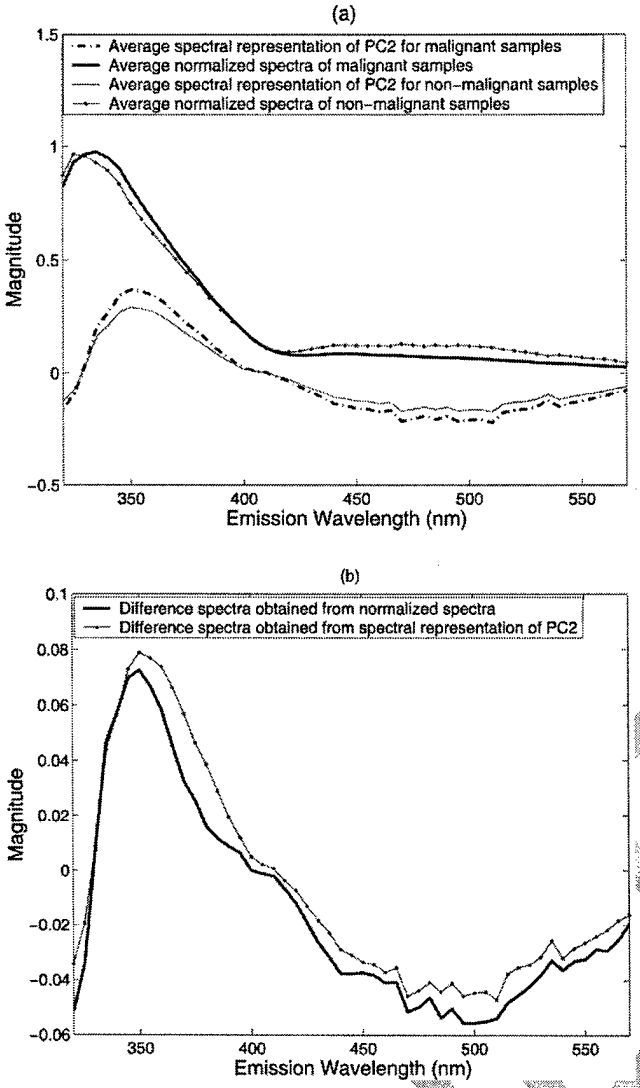

Fig. 4. (a) The average normalized fluorescence spectra at 300 nm, excitation, and the average spectral representations reflected by PC2 (which was obtained from the normalized fluorescence spectra at 300 nm, excitation), for malignant and nonmalignant tissues, and (b) the difference spectra (between malignant and nonmalignant tissues) for each case. The spectral representations are re-projections from the PC subspace onto the normalized spectral data space. They are calculated by simply multiplying the PC scores (in this case, PC2) for all samples by the associated eigenvector and then averaging the spectral representations for each tissue type (malignant and nonmalignant). The difference spectrum was obtained by subtracting (point-by-point) the average nonmalignant spectrum from the average malignant spectrum.

of 300 nm is used. Spectral representations obtained from PC4 at 400-nm excitation, and PC3 at 460-nm excitation are not shown here, but indicate that the maximal differences between malignant and nonmalignant tissues are observed at emission wavelengths of 460 and 540 nm, respectively.

IV. Discussion

Optical spectroscopy in the UV-VIS spectral range is demonstrated to be useful in discriminating malignant and nonmalignant human breast tissues. By measuring fluorescence spectra at multiple excitation wavelengths as well as diffuse reflectance spectra and performing a separate analysis on each, those spectra that are most useful in discriminating malignant and nonmalignant tissues were identified. The analysis indicated that only four of the ten measured spectra are required to maximize classification accuracy. These include fluorescence spectra at excitation wavelengths of 300, 400, 420, and 460 nm. This has important implications in clinical applications, where both speed and cost are important, in that the fewer wavelengths that have to be measured, the faster and less complex the instrument can be.

One problem with the particular approach employed here for analysis is that it can be difficult to determine the biologic basis of the differences observed in the fluorescence spectra of malignant and nonmalignant tissues. However, an understanding of the fluorophores that contribute to the fluorescence spectra at the four optimal excitation wavelengths can yield some insight into the sources of endogenous contrast present. The excitation wavelengths used, ranging from 300 to 460 nm, allow for the characterization of a number of fluorophores, including tryptophan, NAD(P)H, flavoproteins and collagen [17]. By using a range of excitation wavelengths, one is able to characterize many or all of the biological fluorophores present in breast tissue. The fluorescence excitation-emission wavelengths identified as being diagnostic from the PCA-SVM algorithm suggest that the important fluorophores for breast cancer diagnosis are tryptophan, collagen, NADH and flavoproteins. This qualitative analysis does not preclude the possibility that the differences in the fluorescence spectra of malignant and nonmalignant tissues may also be influenced by the absorption of hemoglobin.

As discussed previously, the fluorescence spectra at 300 nm, excitation appear to be most diagnostic of breast cancer. Fig. 4 shows a red shift in the fluorescence peak at 340 nm (tentatively assigned to tryptophan fluorescence), and a decrease in fluorescence at the smaller peak occurring around 450-nm emission (tentatively assigned to NADH fluorescence) in the malignant samples, relative to nonmalignant tissues. This finding is consistent with previous work by Yang *et al.* [10], who found that at an excitation wavelength of 300 nm, the fluorescence emission peak at 340 nm was red-shifted for malignant samples relative to that of normal adipose tissues and the fluorescence at around 450-nm emission was decreased in malignant relative to fibrous tissues. It may be that the shifted peak is useful in discriminating the malignant tissues from adipose, and that the decreased fluorescence at 450 nm is useful in discriminating malignant tissue from benign fibrous tissues, and so the combination of the two features makes this particular PC useful in discriminating malignant and nonmalignant tissues.

Diffuse reflectance can characterize some of the same optical features exploited in fluorescence spectroscopy, notably absorption due to various biological chromophores, and tissue scattering properties. The primary absorbers are oxygenated and deoxygenated hemoglobin, which are present in blood. These compounds, which have slightly different absorption spectra, can be used as an indicator of tissue oxygenation [17]. β-carotene is another chromophore and is present in adipose tissues, thus providing a unique indicator of this tissue type. The primary advantage of this technique is that diffuse reflectance signals are several orders of magnitude greater than the weak endogenous fluorescence signals measured from tissue. Therefore, if diffuse reflectance measurements were

capable of discriminating malignant and nonmalignant tissues at similar accuracies to that of fluorescence measurements, there would be a considerable increase in cost-effectiveness. However, using a similar classification technique, diffuse reflectance spectroscopy was not capable of discriminating between malignant and nonmalignant tissues with the same accuracy as fluorescence spectroscopy. Therefore, there is an apparent advantage to using fluorescence in addition to, or instead of diffuse reflectance. This advantage is likely due to the additional chemical specificity that arises from the fluorescence characterization of the many biologic fluorophores intrinsically present in tissue.

Bigio *et al.* reported better classification accuracies for discriminating between malignant and nonmalignant breast tissues using diffuse reflectance spectroscopy in a pilot study [16], as well as in a more recently published abstract [25]. However, it is difficult to compare classification accuracies achieved in our study to that carried out by Bigio and co-workers due to differences in the clinical protocol (the studies by Bigio and co-workers were carried out on tissues *in vivo*), probe geometry, spectral range (the spectral measurements were made from 330–750 nm) and methods of analysis employed in the two studies. What can be concluded from the work presented here is that fluorescence spectroscopy provides superior classification accuracy compared to diffuse reflectance spectroscopy when evaluated on the same samples using the same methods of analysis.

A novel nonparametric algorithm was developed to identify and incorporate the optimal spectral features for discriminating between malignant and nonmalignant breast tissues. The use of the Wilcoxon test and SVM classification scheme does not require a priori knowledge about the sample distribution and thus, can be utilized for the analysis of small sample sizes. Cross-validation of the algorithm highlights the importance of obtaining an unbiased estimate of the algorithm's classification accuracy. Cross-validation techniques may indicate that the training data set is not sufficient to fully characterize the variance of each subgroup (malignant and nonmalignant tissues). Thus, by removing one data point, the decision hyperplane is altered enough to misclassify some additional samples. Indeed, in examining the misclassified samples, it is clear that some underrepresented sub-groups of tissue types are most frequently misclassified. There were five malignant samples that were consistently misclassified (once in cross validation and repeatedly in the training set). Of these five samples two were carcinoma *in situ* (CIS) and two were lobular cancers. These samples represent the total number of CIS and lobular cancers in the entire sample pool. Upon cross-validation, one of these samples would be removed prior to training the algorithm, leaving just one other sample of this type to aid in its classification. Thus the total variance accounted for by these types of cancers is not well represented in the training set, which results in the frequent misclassification of these particular cancers. Upon the inclusion of more data points from these sample types, the unbiased (testing) classification accuracy may approach the accuracy achieved with the training data set.

Typically, the optical spectral features of different tissue types are not fully separable, which gives rise to imperfect classification. The classification accuracy is also dependent on the algorithm used. Given a constant sample size, one approach to improving the classification accuracy may be to incorporate more features into the classifier (such as PCs). As depicted in Table IV, increasing the number of inputs did not significantly improve the classification accuracy. An alternative approach to improving the classification accuracy is to use nonlinear rather than the linear methods of analysis employed here, i.e., PCA and linear SVM. For example, using a nonlinear kernel in SVM classification may improve the classification accuracy, since the nonlinear kernel SVM is expected to be superior to the linear kernel in dealing with nonseparable cases. This is beyond the scope of the current study, but will be explored in future investigations.

One of the goals of future work is to carry out clinical studies to explore the effectiveness of optical spectroscopy for detecting breast cancer during core needle biopsy. In particular, side-firing fiber-optic probes will be designed and fabricated for use in a Mammatome core biopsy needle. The tip of the needle has a side-facing aperture (19 mm long and 2 mm wide), through which pieces of tissue can be vacuum suctioned when the needle is inserted into the breast. The side-firing probes can be incorporated into the needle to measure fluorescence and diffuse reflectance spectra of breast tissues after the needle is positioned in the area of concern in the breast, but before biopsy. The diagnosis based on the spectral features can be compared to histology of the corresponding biopsy to evaluate the diagnostic potential of this technique.

It would also be desirable to gain a quantitative understanding of the biological basis for the observed spectral differences, which are difficult to determine directly from the tissue spectra. As such, the use of systems employing cell lines and tissue cultures are being explored. A stepwise approach to this technology is warranted, starting with simple systems and adding additional levels of complexity. For example, a normal and malignant cell monolayer could first be imaged to establish the intrinsic fluorescence properties of these cell types. Then the same cells could be grown in a 3-D collagen matrix, adding the effects of the interaction with the extracellular matrix. Finally, these cells could be implanted into nude mice models to explore the added effects of the vasculature and adipose tissue. Such a stepwise approach could allow one to compare simpler, better understood models to what has been characterized in tissue, and could perhaps allow one to determine what tissue constituent is most responsible for the observed spectral differences. This is a promising avenue of research, and applied to the breast could allow for an increased understanding of the underlying mechanism for how optical spectroscopy is able to diagnose this disease.

REFERENCES

[1] J. R. Harris, M. E. Lippman, M. Morrow, and C. K. Osborne, *Diseases of the Breast*, 2nd ed. Philadelphia, PA: Lippicott Williams & Wilkins, 2000.

[2] R. J. Jackman, K. W. Nowels, J. Rodriguez-Soto, F. A. Marzoni Jr, S. I. Finkelstein, and M. J. Shepard, "Stereotactic, automated, large-core needle biopsy of nonpalpable breast lesions: False-negative and histologic underestimation rates after long-term follow-up," *Radiology*, vol. 210, no. 3, pp. 799–805, 1999.

[3] D. D. Dershaw, E. A. Morris, L. Liberman, and A. F. Abramson, "Nondiagnostic stereotaxic core breast biopsy: Results of rebiopsy," *Radiology*, vol. 198, no. 2, pp. 323–5, 1996.

[4] J. E. Meyer, D. N. Smith, S. C. Lester, P. J. DiPiro, C. M. Denison, S. C. Harvey, R. L. Christian, A. Richardson, and W. D. Ko, "Large-needle core biopsy: Nonmalignant breast abnormalities evaluated with surgical excision or repeat core biopsy," *Radiology*, vol. 206, no. 3, pp. 717–720, 1998.

[5] N. Ramanujam, "Fluorescence spectroscopy of neoplastic and nonneoplastic tissues," *Neoplasia*, vol. 2, no. 1–2, pp. 89–117, 2000.

[6] S. K. Majumder, P. K. Gupta, B. Jain, and A. Uppal, "UV excited autofluorescence spectroscopy of human breast tissues for discriminating cancerous tissue from benign tumor and normal tissue," *Lasers Life Sci.*, vol. 8, no. 4, pp. 249–264, 1999.

[7] P. K. Gupta, S. K. Majumder, and A. Uppal, "Breast cancer diagnosis using N2 laser excited autofluorescence spectroscopy," *Lasers Surg. Med.*, vol. 21, no. 5, pp. 417–242, 1997.

[8] Y. Yuanlong, E. J. Celmer, M. Zurawska-Szczepaniak, and R. R. Alfano, "Excitation spectrum of malignant and benign breast tissues: A potential optical biopsy approach," *Lasers Life Sci.*, vol. 7, no. 4, pp. 249–265, 1997.

[9] Y. Yang, A. Katz, E. J. Celmer, M. Zurawska-Szczepaniak, and R. R. Alfano, "Fundamental differences of excitation spectrum between malignant and benign breast tissues," *Photochem. Photobiol.*, vol. 66, no. 4, pp. 518–522, 1997.

[10] ——, "Optical spectroscopy of benign and malignant breast tissues," *Lasers Life Sci.*, vol. 7, no. 2, pp. 115–27, 1996.

[11] R. R. Alfano, A. Pradhan, G. C. Tang, and S. J. Wahl, "Optical spectroscopic diagnosis of cancer and normal breast tissues," *J. Opt. Soc. Amer. B (Opt. Phys.)*, vol. 6, no. 5, pp. 1015–1023, 1989.

[12] R. R. Alfano, G. C. Tang, A. Pradhan, W. Lam, D. S. J. Choy, and E. Opher, "Fluorescence spectra from cancerous and normal human breast and lung tissues," *IEEE J. Quantum Electron.*, vol. QE-23, pp. 1806–1811, Oct. 1987.

[13] Y. Yang, E. J. Celmer, J. A. Koutcher, and R. R. Alfano, "UV reflectance spectroscopy probes DNA and protein changes in human breast tissues," *J. Clin. Laser Med. Surg.*, vol. 19, no. 1, pp. 35–39, 2001.

[14] N. Ghosh, S. K. Mohanty, S. K. Majumder, and P. K. Gupta, "Measurement of optical transport properties of normal and malignant human breast tissue," *Appl.-Optics*, vol. 40, no. 1, pp. 176–84, 2001.

[15] S. V. Pushkarev, S. A. Naumov, S. M. Vovk, V. A. Volovodenko, and V. V. Udut, "Application of laser fluorescence spectroscopy and diffuse reflection spectroscopy in diagnosing the states of mammary gland tissue," *Optoelectron., Instrum. Data-Processing*, vol. 2, pp. 71–76, 1999.

[16] I. J. Bigio, S. G. Bown, G. Briggs, C. Kelley, S. Lakhani, D. Pickard, P. M. Ripley, I. G. Rose, and C. Saunders, "Diagnosis of breast cancer using elastic-scattering spectroscopy: Preliminary clinical results," *J. Biomed. Opt.*, vol. 5, no. 2, pp. 221–228, 2000.

[17] N. Ramanujam, "Fluorescence spectroscopy in vivo," in *Encyclopedia of Analytical Chemistry*, R. Meyers, Ed. New York: Wiley, 2000, pp. 20–56.

[18] Y. Yang, E. J. Celmer, J. A. Koutcher, and R. R. Alfano, "DNA and protein changes caused by disease in human breast tissues probed by the Kubelka-Munk spectral functional," *Photochem. Photobiol.*, vol. 75, no. 6, pp. 627–632, 2002.

[19] G. M. Palmer, C. L. Marshek, K. M. Vrotsos, and N. Ramanujam, "Optimal methods for fluorescence and diffuse reflectance measurements of tissue biopsy samples," *Lasers Surg. Med.*, vol. 30, no. 3, pp. 191–200, 2002.

[20] Q. Liu, C. Zhu, and N. Ramanujam, "Experimental validation of Monte Carlo modeling of fluorescence in tissues in the UV-visible spectrum," *J. Biomed. Opt.*, vol. 8, 2003.

[21] J. A. Welch and J. C. M. Van Gemert, *Optical-Thermal Response of Laser-Irradiated Tissue*. New York: Plenum, 1995.

[22] R. A. Johnson and D. W. Wichern, *Applied Multivariate Statistical Analysis*. Englewood Cliffs, N.J: Prentice-Hall, 1982.

[23] R. M. Bethea, B. S. Duran, and T. L. Boullion, *Statistical Methods for Engineers and Scientists*, 3rd ed., M. Dekker, Ed. New York, 1995.

[24] C. Burges, "A tutorial on support vector machines for pattern recognition," *Data Mining and Knowledge Discovery*, vol. 2, no. 2, pp. 121–167, 1998.

[25] A. C. Lee, C. D. O. Pickard, M. R. S. Keshtgar, G. M. Briggs, M. Falzon, S. Lakhani, I. Bigio, and S. G. Bown, "Elastic scattering spectroscopy for the diagnosis of breast cancer," *Br. J. Surg.*, vol. 89, no. Suppl. 1, pp. 74–74, 2002.

Gregory M. Palmer is a graduate student in the Department of Biomedical Engineering at the University of Wisconsin, Madison. He received the B.S. degree in biomedical engineering from Marquette University, Milwaukee, WI, in June, 2000, and the M.S. degree from the University of Wisconsin, Madison, in December 2002. He is presently working toward his doctorate at the same school.

Mr. Palmer is a member of SPIE.

Changfang Zhu received the B.S. degree in biomedical engineering from the Zhejiang University, Hangzhou, China, in 1998, and the M.S. degree in biomedical engineering from Tsinghua University, Beijing, China, in 2001. She is currently working towards the Ph.D. degree in electrical engineering at the University of Wisconsin, Madison.

Ms. Zhu is a member of the SPIE.

Tara M. Breslin is an Assistant Professor in the Section of Surgical Oncology at the University of Wisconsin Medical School, Madison. Her research interests include clinical trials in breast cancer technology and development in breast cancer diagnosis and treatment.

Dr. Breslin is a member of the Society of Surgical Oncology, the Fellow American College of Surgeons, and the American College of Surgeons Oncology Group.

Fushen Xu is an Instructor with the Department of Pathology and Laboratory Medicine at the University of Wisconsin Medical School, Madison.

Kennedy W. Gilchrist is a Professor of Pathology and Laboratory Medicine at the University of Wisconsin Medical School, Madison. His primary research interests involve aspects of breast cancer care.

Dr. Gilchrist is a member of the Eastern Cooperative Oncology Group, and is on the Editorial Board of *Breast Cancer Research and Treatment.*

Nirmala Ramanujam received the Ph.D. degree in biomedical engineering from the University of Texas, Austin, in 1995. Her area of specialization was in biomedical optical spectroscopy.

She was awarded the National Research Service Award from the NIH to do a Postdoctoral fellowship at the University of Pennsyslania (UPENN), Philadelphia, and following this fellowship, she worked as an Assistant Professor in the Department of Biochemistry and Biophysics at UPENN. In 2000, she joined the University of Wisconsin, Madison, as an Assistant Professor of Biomedical Engineering. Her current research interests are centered on developing optical diagnostic modalities for breast cancer.

Dr. Ramanujam is a member of OSA, SPIE, APS, ASLMS, and ASEE.